

UNCLASSIFIED
RESTRICTED

Copy No.

RM No. A9B17



3 1176 00078 8985

CHANGED

41155

NACA RM No. 41155

~~UNCLASSIFIED~~
NACA

authored by *H. L. Dryden et al - 11-53*
per NACA Release form #1488. By H-AR, 7-21-53

RESEARCH MEMORANDUM

CHORDWISE AND SPANWISE LOADINGS MEASURED AT LOW
SPEED ON LARGE TRIANGULAR WINGS

By Adrien E. Anderson

Ames Aeronautical Laboratory
Moffett Field, Calif.

~~FOR REFERENCE~~

~~NOT TO BE TAKEN FROM THIS ROOM~~

CLASSIFIED DOCUMENT

This document contains classified information affecting the National Defense of the United States within the meaning of the Espionage Act, USC 50131 and 50. Its transmission or the revelation of its contents in any manner to an unauthorized person is prohibited by law. Information so classified may be imparted only to persons in the military and naval services of the United States, appropriate civilian officers and employees of the Federal Government who have a legitimate interest therein, and to United States citizens of known loyalty and discretion who of necessity must be informed thereof.

**NATIONAL ADVISORY COMMITTEE
FOR AERONAUTICS**

WASHINGTON
April 19, 1949

~~RESTRICTED~~

UNCLASSIFIED

NACA RM No. A9B17

NATIONAL ADVISORY COMMITTEE FOR AERONAUTICS

RESEARCH MEMORANDUM

CHORDWISE AND SPANWISE LOADINGS MEASURED AT LOW
SPEED ON LARGE TRIANGULAR WINGS

By Adrien E. Anderson

SUMMARY

Pressure distributions have been obtained from three triangular wing models: a wing-alone model having an aspect ratio of 2.04 and a modified double-wedge airfoil section, the same wing combined with a body of fineness ratio 12.5, and a mock-up of a triangular-wing airplane which had an aspect ratio of 2.31 and an NACA 65-006.5 airfoil section. Pressure data were obtained through an angle-of-attack range at zero angle of sideslip. The Reynolds number as based on the mean aerodynamic chord, was approximately 15×10^6 at a corresponding Mach number of 0.13.

Chordwise pressure distributions, section lift coefficients, and section centers of pressure are presented for several spanwise stations and angles of attack. Span load distributions are also included.

Comparison of the results on the several configurations indicated that similarity among the corresponding wing characteristics (the chordwise distribution of pressure and the nearly elliptic spanwise loading) occurred only at the lower angles of attack where essentially inviscid potential flow existed on the wings. In the middle angle-of-attack range, the aerodynamic characteristics of the three wings differed. Leading-edge separation, which occurred on the tip sections first and then progressed inboard, appeared to be dependent upon the curvature of the forward portion of the airfoil section - the sharper the nose section, the earlier the separation. Leading-edge separation resulted in a form of air flow which produced abrupt changes in the section characteristics, but only negligible changes in the integrated wing characteristics. At angles of attack near wing stall the corresponding wing-section characteristics for the models were again very similar.

UNCLASSIFIED

It was inferred from the data that the body carried a lift approximately equal to the lift which would be carried by the wing area it covered.

INTRODUCTION

Although low-aspect-ratio wings of triangular plan form are primarily intended for use at supersonic speeds, the designer of an airplane employing this wing design is also concerned with their low-speed characteristics. With regard to the low-speed pressure distribution on triangular wings of aspect ratio 2, reference 1 reported the results of an investigation on a triangular wing with a subsonic-type airfoil section of moderate thickness (NACA 0012). Due to the interest in wings having thinner sections, it was considered desirable to investigate the low-speed pressure distribution on a wing having the same plan form and aspect ratio but a supersonic-type airfoil section.

In addition, an appropriate supersonic-type body was added to the wing to determine the effect of a body on the loading of a triangular plan-form wing of low aspect ratio. Finally, the mock-up of a triangular-wing airplane of approximately the same aspect ratio, but having a thin low-drag subsonic-type airfoil section (NACA 65-006.5), was made available to the NACA for investigation.

The results of the pressure-distribution investigation on these large-scale models have been summarized in this report in order to make the much needed data available to designers of aircraft with wings of triangular plan form. This report, then, in conjunction with reference 1, makes available a comparison of the loading on two triangular wings, one having a relatively thick subsonic-type and the other a thin supersonic-type airfoil section. In addition, the data presented in this report indicate the effect of a body on the wing load distribution as well as providing a qualitative comparison of the loadings on two wing-body combinations, one having a thin subsonic-type and the other a thin supersonic-type airfoil section.

SYMBOLS AND COEFFICIENTS

The symbols and coefficients used in this report are defined as follows:

A aspect ratio $\left(\frac{b^2}{S} \right)$

α free-stream angle of attack of wing chord plane, degrees

- b wing span, feet
- c wing chord, measured parallel to air stream, feet
- c_{av} average wing chord (S/b), feet
- \bar{c} mean aerodynamic chord, measured parallel to air

$$\text{stream} \left(\frac{\int_0^{b/2} c^2 dy}{\int_0^{b/2} c dy} \right), \text{ feet}$$

- c_l section lift coefficient $\left(\frac{\text{section lift}}{qc} \right)$

- C_L wing lift coefficient $\left(\frac{\text{lift}}{qS} \right)$

- C_M wing pitching-moment coefficient about $0.25\bar{c}$ $\left(\frac{\text{pitching moment}}{qS\bar{c}} \right)$

- c_n section normal-force coefficient $\left(\frac{\text{section normal force}}{qc} \right)$

- $\frac{c_l c}{C_L c_{av}}$ span loading coefficient

- P free-stream static pressure, pounds per square foot

- P_l local static pressure, pounds per square foot

- P pressure coefficient $\left(\frac{P_l - P}{q} \right)$

- q free-stream dynamic pressure, pounds per square foot

- S wing area, square feet

- x distance along chord from leading edge, feet

- x_f distance along fuselage center line from nose, feet

- y distance along wing semispan to chord location, feet

EQUIPMENT AND TESTS

The three models used in this investigation were:

1. A wing model, hereafter referred to as the modified-wedge wing, which had a triangular plan form and an aspect ratio of 2.04. The airfoil section parallel to the wing center line was derived from a symmetrical double-wedge section having a maximum thickness of 5-percent chord at 20-percent chord. The modification consisted of a 0.0025c nose radius and a rounded maximum thickness formed from an arc (0.62c radius) which was tangent to the surface of the double wedge at 15- and 25-percent chord. Both the top and bottom of the section were rounded. In terms of the resultant chord, the airfoil section had a nose radius of 0.00254c and a thickness of 4.83 percent at 21.6-percent chord. This was the same wing for which force data were presented in reference 2.

2. A modified-wedge wing-body model, which consisted of the above-mentioned wing combined with a slender and pointed body of revolution. The radius r of the body at any station x_f was obtained from the following equation:

$$r = 2.245 \left[1 - \left(1 - \frac{x_f}{28.08} \right)^2 \right]^{3/4}$$

3. A mock-up of a triangular-wing airplane which had an aspect ratio 2.31 and an NACA 65-006.5 airfoil section parallel to the wing center line. This model, which will be referred to as the NACA 65-series wing-body model, was equipped with constant-chord trailing-edge controls. The control had a horn balance, a nose radius, and a small but unsealed gap. The ducting system was open and the power plant removed.

Three-view drawings of the two wing-body models appear in figure 1, while figure 2 contains photographs of the models as mounted for testing in the Ames 40- by 80-foot wind tunnel. Additional dimensional data for the three models and the ordinates of the NACA 65-series airfoil section will be found in tables I and II, respectively.

The pressure orifices, in the case of the modified-wedge wing, were located along chord lines at six spanwise stations in the top and bottom surfaces of the right half of the wing. (See fig. 3(a).) The body used in the modified-wedge wing-body combination covered the pressure orifices along the chord line at the 0.05 semispan

station. In the NACA 65-series wing-body model, the orifices were located in the left half of the wing along a chord line at the wing-body juncture and four lines of constant-percent local span. (See fig. 3(b).) There was a slight deviation of the orifices from this linear distribution as a result of interference of the orifices with the internal structure of the wing.

The pressure data were obtained through the angle-of-attack range at zero angle of sideslip for the three models. An additional run was made on the NACA 65-series wing-body combination with the trailing-edge flap deflected up 10° . The dynamic pressure for the tests was approximately 25 pounds per square foot (Mach number = 0.13) with corresponding Reynolds numbers (based on the mean aerodynamic chord) of 14.3×10^6 for the modified-wedge wing and 16.4×10^6 for the NACA 65-series wing-body combination.

REDUCTION OF DATA

The pressure coefficients, reduced from the measured local static pressures, are believed accurate to within ± 2 percent. The chordwise pressure plots for the modified-wedge wing and wing-body models were obtained directly since the pressure orifices were located along chord lines. However, on the NACA 65-series wing-body model, the fact that the majority of the pressure orifices were not located along chord lines made it necessary to construct preliminary plots of the data (as indicated in fig. 4).

Values of section normal-force coefficient and section center of pressure were derived from the chordwise pressure plots by means of mechanical integration and calculation. The values of section lift coefficients do not include the effects of the forces parallel to the chord. Representative calculations of the chordwise forces indicated a maximum increase of only 2 percent in the section lift coefficients.

When the NACA 65-series wing-body model data are taken into consideration, the lack of pressure orifices near the leading edge and the wing tip makes the nature of the data somewhat questionable in these regions. On the other hand, an integration for $\alpha = 8.3^\circ$ of the section normal forces plus an approximation of the force on the fuselage gave a value of C_L which was only 8 percent less than the force test C_L . With such agreement it is reasonable to expect that the results for the NACA 65-series wing-body model are also of sufficient accuracy to be indicative of general trends.

The values of wing lift coefficient used in computing the span-loading coefficients were obtained from the force-test lift curves of figure 5. The use of lift-coefficient values from the force test was necessary since the pressures on the body were not determined.

The values of the angle of attack of the wing have been corrected for air-stream inclination and for wind-tunnel-wall effect, the latter correction being that for a wing of the same span and having elliptic loading, but with an unswept plan form.

RESULTS AND DISCUSSION

Separation-Vortex Air Flow Over Triangular Wings

In reference 2 it was reported that, on certain occasions during the force-test investigation of the wing with double-wedge section, condensation trails appeared revealing the presence of two vortices extending downstream somewhat in the manner shown in figure 6(a). The vortices, which resulted when the separated flow off the sharp leading edge coalesced, first appeared at an angle of attack corresponding to a wing lift coefficient of approximately 0.6. No condensation trails were ever noticed at the lower angles of attack, or when the wing leading edge was rounded. This lack of vapor trails did not necessarily indicate the nonexistence of the vortices; they may have been weaker.

During the investigation reported herein, vapor trails did not appear on any of the models. In the case of the modified-wedge wing model, however, their presence was detected by means of a survey of the flow above the wing. Their presence is also apparent in the chordwise pressure plots for the modified-wedge wing and wing-body models. There is some evidence in the pressure plots for the NACA 65-series wing-body model to indicate that separation vortices may have existed on this model also. An understanding of the pattern of this vortex type of flow will aid in the interpretation of the results of this investigation.

The following description of the formation of the separation vortices is based on the visual observation of vapor trails on the wedge wing (reference 2) and the survey of the flow above the modified-wedge-wing model. The vortex, considering one-half of the wing at a time, originated first on the leading edge near the wing tip, following separation of the flow in this region. Line A of figure 6(b) represents the vortex pattern for $\alpha = 3^\circ$. Increasing the angle of attack caused the point of origin of the vortex to move

forward along the leading edge toward the apex of the wing until the point of origin reached the apex at about $\alpha = 8^\circ$. The angle of sweepback of the vortex increased with angle of attack, the rate of increase being largest at the lower angles of attack of the wing. Also, at the lower angles, that portion of the vortex lying over the outer 30 percent of the wing span was bent back slightly toward the free stream. The latter condition is represented by line B of figure 6(b). At an angle of attack of about 18° , the angle of sweepback of the vortex seemed fairly well established and apparently the strength of the vortex began to diminish toward the apex (the vapor trails of fig. 6(a) or line C of fig. 6(b)). By the time the wing had stalled, all evidence of the vortex had disappeared.

General Comments

Comparison of the results of this investigation with those for the wing with NACA 0012 airfoil section (reference 1) indicated that some generalities exist concerning the wing characteristics which should be kept in mind throughout the discussion to follow. Similar pressure distributions occurred over the wings only at the lower angles of attack where essentially inviscid potential flow existed on the wings. The pressure distributions became dissimilar in the middle angle-of-attack range following flow separation from the leading edge. The occurrence of leading-edge separation and the intensity of the resultant vortex-type flow appeared to be dependent upon the airfoil section. The modified-wedge wing and wing-body models showed signs of leading-edge separation first and a stronger effect of the vortex-type flow. In the case of the NACA 65-series wing-body model, separation was delayed and the effect of the vortex less strong. It is difficult to conclude from the pressure diagrams for the model with NACA 0012 sections (reference 1) if the vortex-type flow was present. The minor bumps in the pressure diagrams make it appear likely that this model had a very weak vortex-type flow. At angles of attack near wing stall, where the influence of the vortex-type flow had become negligible, the characteristics of the three models were nearly similar. In general, the characteristics of the NACA 65-series wing-body model more closely resembled those for the model with NACA 0012 section than those for the two models with modified-wedge sections.

Chordwise Pressure Distribution

The chordwise pressure diagrams for the modified-wedge-wing model are presented in figure 7. Whereas data were obtained at very

small increments of angle of attack on the modified-wedge wing and wing-body models, results are presented for only those angles for which the pressure diagrams are indicative of the general changes in loading on the wing. The section loading increased toward the wing tip at the very low angles of attack, that is, up to 4.2° , when essentially inviscid potential flow existed on the wing. High tip loading at low angles of attack was a characteristic of the NACA 0012 wing (reference 1). However, the tip sections of the modified-wedge wing stalled at much lower angles of attack, which was quite likely due to the relatively small nose radius and the abrupt change of curvature which results at the juncture of the nose radius and the sides of the wedge, in contrast to the smooth transition on the NACA 0012 section.

The first signs of leading-edge separation are found in the chordwise pressure distribution for the 0.9-semispan station at an angle of attack of 4.2° (fig. 7(c)) where the value of the negative pressure at the leading edge has decreased slightly from that for the previous angle of attack and there is a nearly uniform negative pressure area extending over the forward half of the chord length. As the angle of attack was increased, the separated flow area moved progressively inward as indicated by the chordwise extent of the nearly uniform negative pressure area on the inboard sections.

The separation of the flow did not result in a subsequent loss in load on the section. Any loss in load as a result of a loss in peak nose pressure was counteracted by an increase due to the low-pressure bumps in the chordwise pressure diagrams, which resulted when the separated flow gradually formed the previously described vortices. While these bumps first appear in the pressure diagrams for the outboard stations at the low angles of attack, they are more apparent over the major portion of the wing at an angle of attack of 14.5° . (See fig. 7(e).) When the diagrams of this figure are redrawn with the abscissa proportional to the local chord length, as has been done in figure 8, the trace of the vortices over the wing becomes even more apparent. In this figure, positive pressure-coefficient values are omitted.

The bending back of the outer portion of the vortices is indicated by the rapid rearward shift of the bump on the pressure diagrams for the 0.75-semispan station through the angle-of-attack range between 4.2° and 14.5° . The effect of the decrease in vortex strength is found in the pressure diagrams for the inboard stations at the higher angles of attack where the reduction in the size of the bumps is more pronounced. For example, notice the formation and the subsequent reduction of the low-pressure bump at the 0.45-semispan

station. At $\alpha = 8.3^\circ$ (fig. 7(d)) separation has taken place and the vortex has formed. In figure 7(e) the bump has increased both pressurewise and chordwise. Near $\alpha = 20.8^\circ$ (fig. 7(f)) the bump has begun to diminish in size and is no longer apparent at $\alpha = 26.9^\circ$ (fig. 7(g)) as a result of the vortex diminishing.

The pattern of the chordwise loading at maximum lift (fig. 7(h)) is very similar to that for the wing with NACA 0012 section (reference 1). The pressure diagrams for the stations outboard of 0.60 semispan indicate complete separation, with the negative pressure values increasing toward the root. The diagrams for the inboard stations give indication of various degrees of separated flow, with the most inboard station having the least signs of separated flow.

The pressure-distribution curves for the modified-wedge wing-body model are presented in figure 9. The primary effect of adding the body was to shift the origin of the separation vortices outboard. The outward shift of the vortices is more clearly seen by comparing the pressure curves for the wing-body combination (fig. 10) with the wing-alone pressure curves at the same angle of attack. (See fig. 8.) Although the bumps on the inboard stations had a more negative pressure peak, they extended over a shorter chord distance, the net result being a reduction in lift on the inboard stations as compared to the wing-alone model.

The chordwise pressure-distribution curves for the NACA 65-series wing-body model are presented in figure 11. In general, the pressure diagrams for this model closely resemble those for the NACA 0012 wing (reference 1). The chordwise distribution of pressure and the value of the wing lift coefficient at which separation occurs on a given section are similar. At the 0.60-semispan station, for example, the pressure diagrams agree closely at the low angles of attack and probably would show closer agreement in the middle range of angle of attack had it been possible to record pressures at the very leading edge of the NACA 65-series wing. At maximum lift, the corresponding pressure diagrams for the two wings are again very similar.

The data outboard of the 0.60-semispan station on the NACA 65-series wing-body model are open to question because of the previously mentioned scarcity of pressure orifices. For example, the pressure diagrams for the 0.90-semispan station give the impression that separated flow existed even at the very lowest angles, which is probably not the case. Following complete separation, however, the pressure diagrams for the 0.90-semispan station resemble those for the modified-wedge-wing model and the values of the section lifts compare favorably. It seems logical to surmise then that, at angles of attack

greater than 12° , the 0.90-semispan-station diagrams are indicative of the actual chord loading.

The discontinuities which appear on the pressure diagram aft of the 0.5-chord station are the pressures at the control-surface slot and not the previously mentioned bumps due to the separation vortex. There is some evidence in the pressure diagrams which indicates the presence of a vortex. The pressure diagrams for the 0.45-, 0.60-, and 0.75-semispan stations in the angle-of-attack range between 8.3° and 20.8° (figs. 11(c) through (e)) have negative pressure peaks which move aft and broaden out with angle of attack. These peaks do not appear to be as extensive or as high as those on the modified-wedge-wing model. It is believed, therefore, that a vortex-type flow did exist, but it was one which was somewhat less intense than on the models with the modified-wedge airfoil section.

The close resemblance of the NACA 65-series wing and the NACA 0012 wing data seems to indicate that the rate of change of curvature of the section near the leading edge, as well as the nose radius and thickness of the section, has a large influence on leading-edge separation. Consider the values of nose radius and thickness for the three sections under discussion:

<u>Section</u>	<u>Maximum thickness percent chord</u>	<u>Nose radius percent chord</u>
NACA 0012	12.0	1.58
Modified wedge	4.8	.25
NACA 65 ₁ -006.5	6.5	.28

It seems unlikely that the small differences in thickness and nose radius could account for the large differences between the pressure diagrams for the modified wedge and the NACA 65-series sections. The more probable factor is the rate of change of curvature of the forward portion of the airfoil section.

Comparison of the pressure-distribution diagrams for the NACA 65-series wing-body combination, having the trailing-edge controls deflected up 10° (fig. 12), with those for controls neutral (fig. 11) at the same angle of attack indicates the normal type of shift of the loading on the aft portion of the section chord.

Section Lift Characteristics

The variation of section lift coefficient with wing angle of

attack is shown in figure 13. As might be anticipated from previous work, the lift curves are nonlinear and the lift-curve slope increases toward the tip. In the case of the modified-wedge wing, the formation of the separation vortex resulted in an appreciable increase in lift on the section, particularly on the outboard stations where the influence of the vortex flow was the strongest. This effect is indicated by the increase in slope of the section lift curves of the outboard stations above an angle of attack of 3° or 4° . It should be remembered that the section lift values are plotted against wing angle of attack. Actually some change in the local induced angle of attack may occur simultaneously with the change in section lift such that, if c_l were plotted against the local angle of attack, there would be no apparent increase in the rate of change of section lift with angle of attack.

Adding the body to the modified-wedge wing resulted in a slight reduction of lift on the inboard stations at a given angle of attack. The cause of this effect is the fact that adding the body shifted the origin of the separation vortices outboard and hence the vortex was weaker for a specific station at the same angle of attack.

The section lift curve for the 0.25-semispan station of the NACA 65-series wing-body model (fig. 13(c)) is nearly coincident with the lift curves for the same station of the modified-wedge wing-body model. At the 0.45, 0.60, and 0.75 stations, however, the curves for the NACA 65-series wing-body model are less steep initially, but do have a rapid rise, the latter occurring at higher angles of attack. Here is evidence pointing not only to the existence of a separation vortex but to its delay to higher angles of attack by use of a subsonic-type airfoil section. The section lift curve for this model at the 0.90-semispan station bears no resemblance to the curve for the modified-wedge wing-body model over the first 12° angle of attack, as would be expected from the previous discussion of the pressure diagrams for this station. At the higher angles, where it is reasonable that complete separation has occurred, the two curves for the 0.90-semispan station agree more closely.

The section lift curves, particularly those for the modified-wedge-wing models, indicate a primary $c_{l_{max}}$ followed by a loss in lift and a subsequent recovery to a secondary $c_{l_{max}}$. In several cases, section lift coefficients for intermediate angles of attack were computed to verify the fairing of the lift curves in the region of the primary $c_{l_{max}}$. The form of the lift curve in the region of the primary $c_{l_{max}}$ appears to be directly related to changes in the vortex pattern. Consequently, the section lift curves fall into three classifications as regards the loss in lift following the

primary $c_{l_{max}}$. The curve for the 0.90-semispan station indicates an abrupt loss in lift as a consequence of the rapid shift of the vortex inward from the tip. In contrast, the curve for the 0.75-semispan station has a nearly flat top as a result of the steady rearward shift of the vortex while maintaining its intensity. On the inboard stations the vortex did not shift appreciably but decreased in intensity slowly, resulting in a lift break which, while extending over a short angle-of-attack range, is not as great as for the outboard stations. Primary $c_{l_{max}}$ points are found in the lift curves for the NACA 65-series wing-body model also.

Were the separation vortex not present or its influence negligible, as on the most inboard stations, no primary $c_{l_{max}}$ would exist and we would find only the secondary $c_{l_{max}}$, or normal section stall. The values of the secondary $c_{l_{max}}$ on these models varied from approximately 0.5 near the tip to as high as 1.6 at the root section indicating a strong three-dimensional effect, for the value of $c_{l_{max}}$ usually associated with thin wing sections is 0.8.

The integrated effect of the section lift was found to be generally smooth with angle of attack as indicated by the curves of lift versus angle of attack for the four models. (See fig. 5.)

The slope through zero lift of the section lift curves of figure 13 has been plotted along the wing span in figure 14. The curve through the points was drawn assuming elliptic loading and an average value of wing lift-curve slope of 0.040 from the force-test data. The close agreement of the section lift values to the theoretical distribution points to the existence of approximately elliptic loading.

Center of Pressure

The chordwise center-of-pressure variation with angle of attack for the models is presented in figure 15. The separation vortices of the modified-wedge-wing model are again noted to have had a strong influence on the section characteristics. The center of pressure on the 0.05-semispan station remained practically constant at about 0.33 x/c . On the next three stations outboard, there was a forward movement of the center of pressure as the vortex flow built up and then a gradual rearward shift as the influence of the vortex decreased. At the 0.75-semispan station, however, the rearward shift of the center of pressure was quite rapid between $\alpha = 4^\circ$ and 10° , as would be expected from the rapid rearward shift of the vortex along the section chord. The shift of the center of pressure was

then forward as the influence of the vortex decreased ($\alpha = 10^\circ$ to 18°). The tip station followed a somewhat similar pattern.

The addition of the body to the modified-wedge wing shifted the origin of the vortex outboard and hence changed the centers of pressure at a given angle of attack. These changes in the centers of pressure were most pronounced at angles of attack above 6° , with the 0.75 and 0.90 stations being least affected.

The rearward shift of the centers of pressure on the NACA 65-series wing body was less abrupt and extended over a shorter chordwise distance. The resultant variation points to the influence of a weaker vortex-type flow than on the modified-wedge-wing models. Deflecting the controls up 10° resulted in a forward shift of the centers of pressure, as would be anticipated.

The integrated effect of the section center-of-pressure variation was found to be generally more gradual with angle of attack, as indicated by the curves of lift coefficient versus pitching-moment coefficient for the four models. (See fig. 5.)

Span Load Distribution

The span-load-distribution curves (fig. 16) were approximately elliptic in shape at low angles of attack for two modified-wedge-wing models. Once the tip section stalled ($\alpha = 4.5^\circ$), there was a progressive shift of the load inboard. As each section stalled, the next section inboard carried a greater load, until ultimately the loading might be described as almost triangular in shape. The addition of the body, as might be expected from the discussion of the section lift curves, shifted the loading outboard slightly at the higher angles of attack. The relatively close agreement of the wing-body span load distributions with those for the wing alone and the close agreement as to the total lift from force test (fig. 5) indicates that the body carried a lift approximately equal to the lift on the wing area which it covers. The distribution of this load along the fuselage, of course, remains to be determined.

It would be anticipated that the loading on the NACA 65-series wing-body model would be nearly elliptic at the lower angles of attack from the fact that the two modified-wedge-wing models and the NACA 0012 wing model had elliptic loading at small angles of attack. However, the span loading curves (fig. 16(c)) do not appear to be elliptic at any angle of attack. This failure to show elliptic loading may be due to the chordwise slot at 83-percent semispan produced

by the horn balance on the control surface or to the deduced values of c_l near the tip being in error due to the previously discussed arrangement of pressure orifices. Some assurance of elliptic loading is found in the spanwise distribution of section-lift-curve slopes (fig. 14) where it will be noted that, except for the 0.90 station, the points representing the section-lift-curve slope for the three models agree quite well.

CONCLUDING REMARKS

Comparison of the results of this investigation with those for the wing with NACA 0012 airfoil section (NACA TN No. 1650, 1948) indicated that some generalities exist concerning the loading characteristics of triangular plan-form wings. Similarity among the corresponding wing characteristics (the chordwise distribution of pressure and the nearly elliptic spanwise loading) occurred only at the lower angles of attack where essentially inviscid potential flow existed on the wings. In the middle angle-of-attack range, the aerodynamic characteristics of the three wings differed. Leading-edge separation, which occurred on the tip sections first and then progressed inboard, resulted in a vortex-type flow. The intensity of the separation vortex and the angle of attack at which it first occurred on the wing appeared to be dependent upon the curvature of the forward portion of the airfoil section. It occurred earliest and most intensely on the wings with the relatively sharp leading edges. The effect of the separation vortex was to produce abrupt changes in the section characteristics, but the effect on the integrated wing characteristics was generally negligible. At the angles of attack near the wing stall, where the effect of the separation vortex was nil, the corresponding section characteristics for the three wings were again very similar.

It was inferred from the data that the body carried a lift approximately equal to the lift which would be carried by the wing area it covered.

Ames Aeronautical Laboratory,
National Advisory Committee for Aeronautics,
Moffett Field, Calif.

REFERENCES

1. Wick, Bradford H.: Chordwise and Spanwise Loadings Measured at Low Speed on a Triangular Wing Having an Aspect Ratio of Two and an NACA 0012 Airfoil Section. NACA TN No. 1650, 1948.
2. Anderson, Adrien E.: An Investigation at Low Speed of a Large-Scale Triangular Wing of Aspect Ratio Two.- II. The Effect of Airfoil Section Modifications and the Determination of the Wake Downwash. NACA RM No. A7H28, 1947.

TABLE I
GEOMETRIC DATA OF MODELS USED IN THE INVESTIGATION

Item	Modified- wedge wing model	Modified- wedge wing- body model	NACA 65- series wing- body model
Wing			
Span, feet	25.00	25.00	31.33
Area, square feet	307	307	425
Area exposed outside of fuselage, square feet	307	211	296
Mean aerodynamic chord, feet	16.37	16.37	18.09
Dihedral, degrees	0	0	0
Angle of incidence, degrees	- - -	0	0
Aspect ratio	2.04	2.04	2.31
Fuselage			
Length, feet	- - -	56.16	41.33
Maximum diameter, feet	- - -	4.49	5.50
Fineness ratio	- - -	12.50	7.52
Maximum diameter wing- span ratio	- - -	0.180	0.176
Trailing-edge control			
Area (total aft of hinge line), square feet	- - -	- - -	76.60
Area (total with horn balance), square feet	- - -	- - -	78.02



TABLE II

NACA 65-006.5 AIRFOIL SECTION ORDINATES

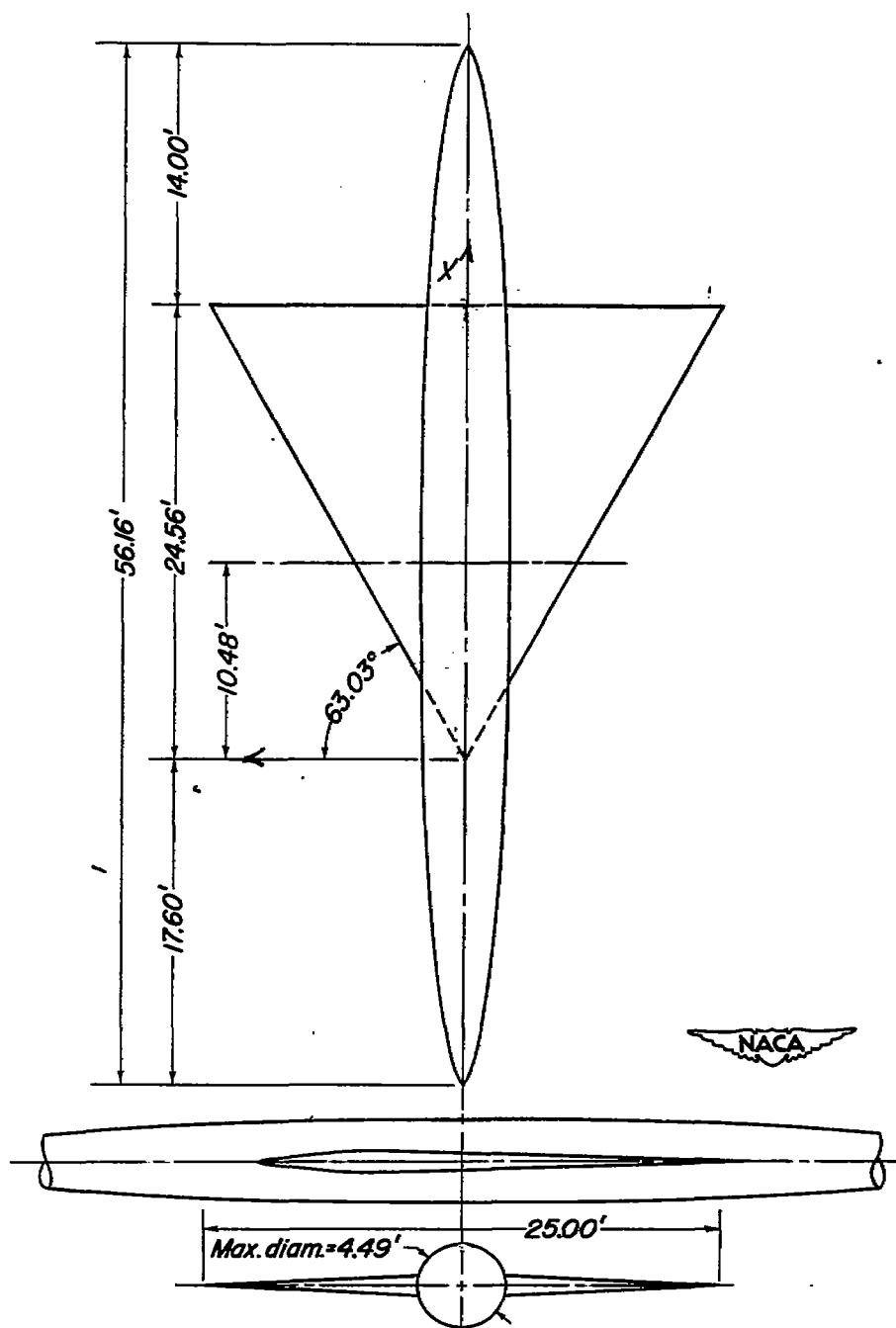
[Stations and ordinates are in percent of airfoil chord]

Station	Ordinates
0	0
.50	± .512
1.25	± .771
2.5	± 1.032
5.0	± 1.415
7.5	± 1.719
10.0	± 1.975
15.0	± 2.379
20.0	± 2.685
25.0	± 2.920
30.0	± 3.087
40.0	± 3.244
50.0	± 3.133
60.0	± 2.719
70.0	± 2.085
80.0	± 1.327
90.0	± .548
95.0	± .210
100.0	0

L. E. radius: 0.282 percent chord

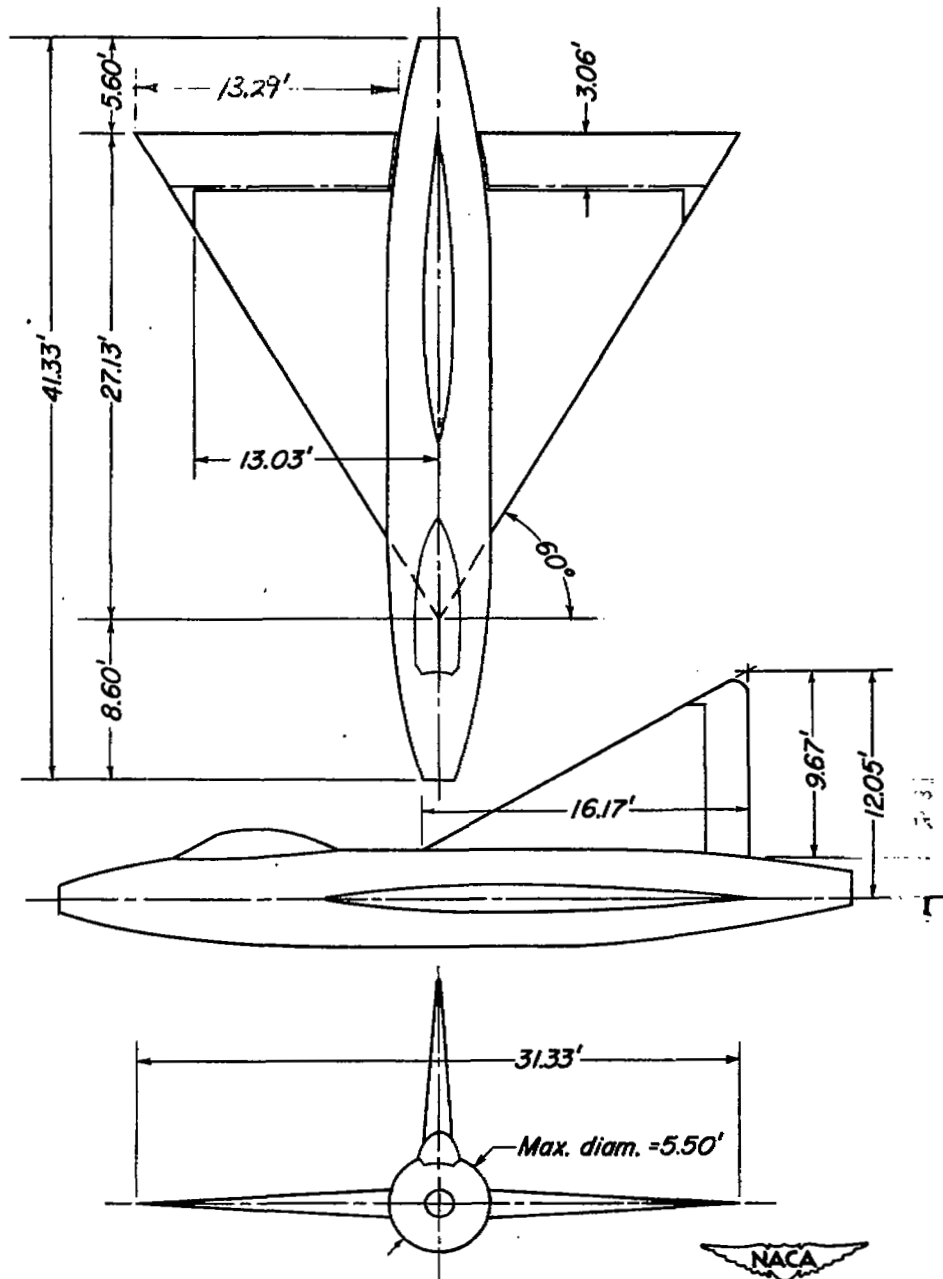






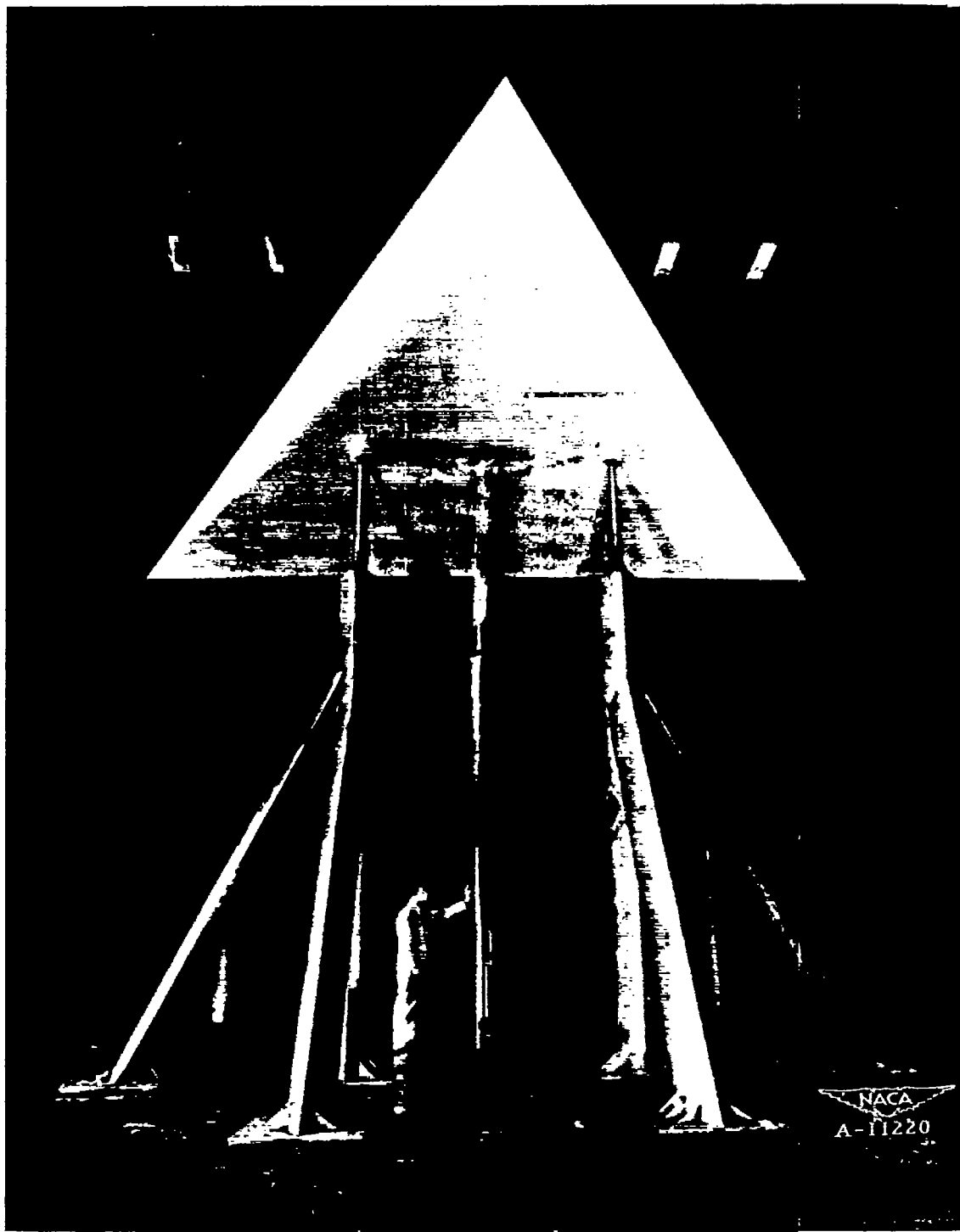
(a) Modified-wedge wing-body model.

Figure 1.- General arrangement of the wing-body models investigated.



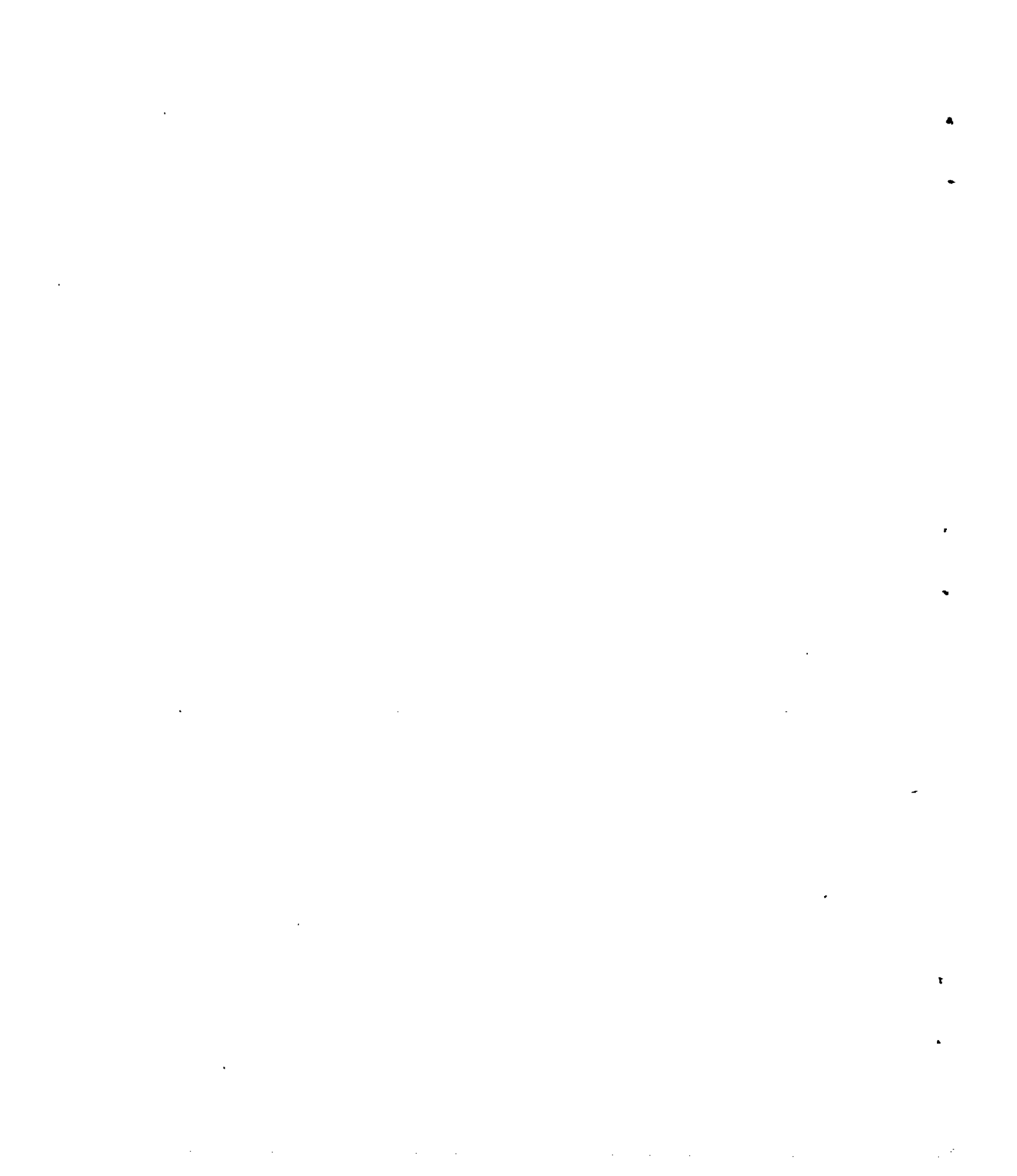
(b) NACA 65-series wing-body model.

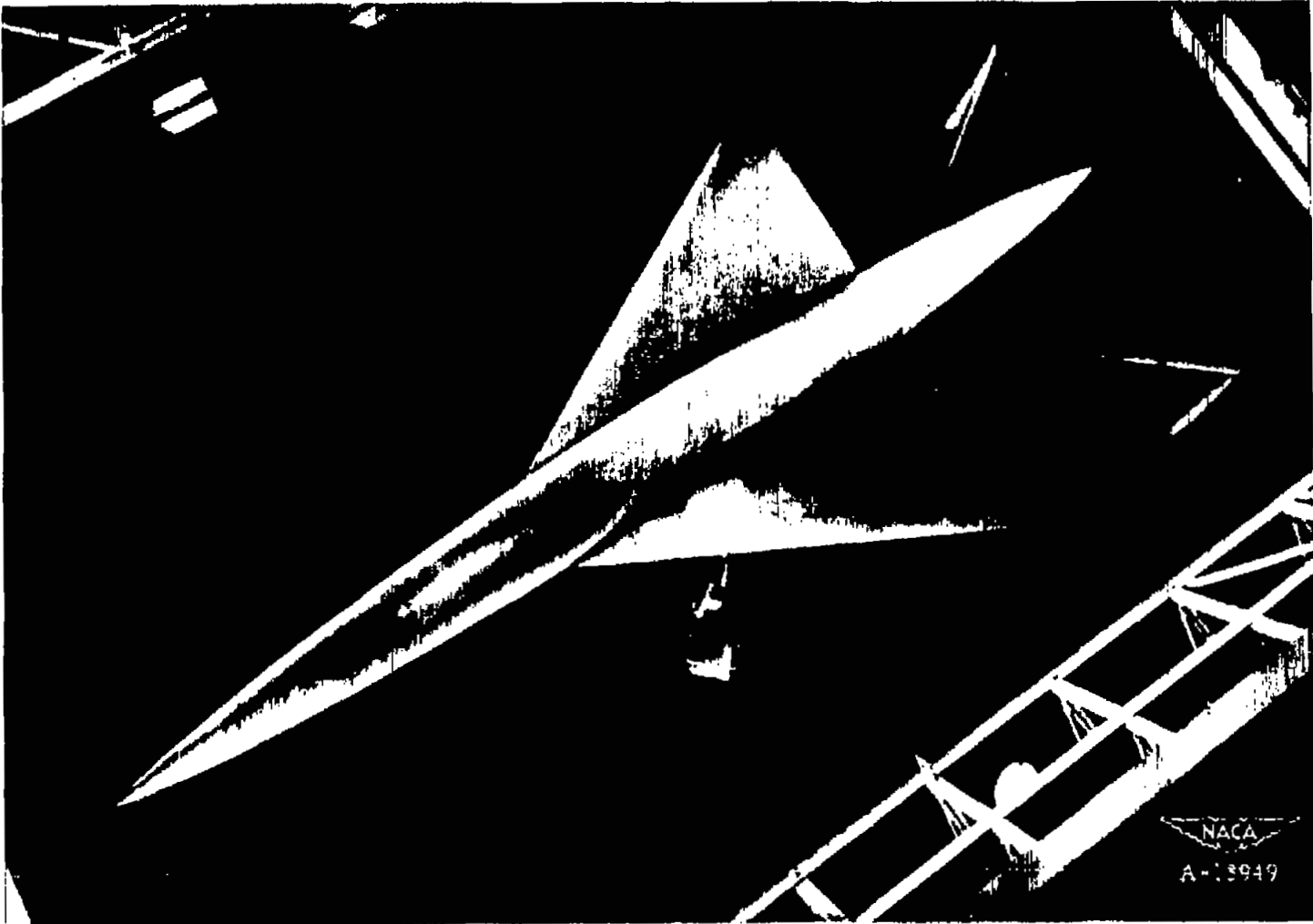
Figure 1.- Concluded.



(a) Modified-wedge wing model.

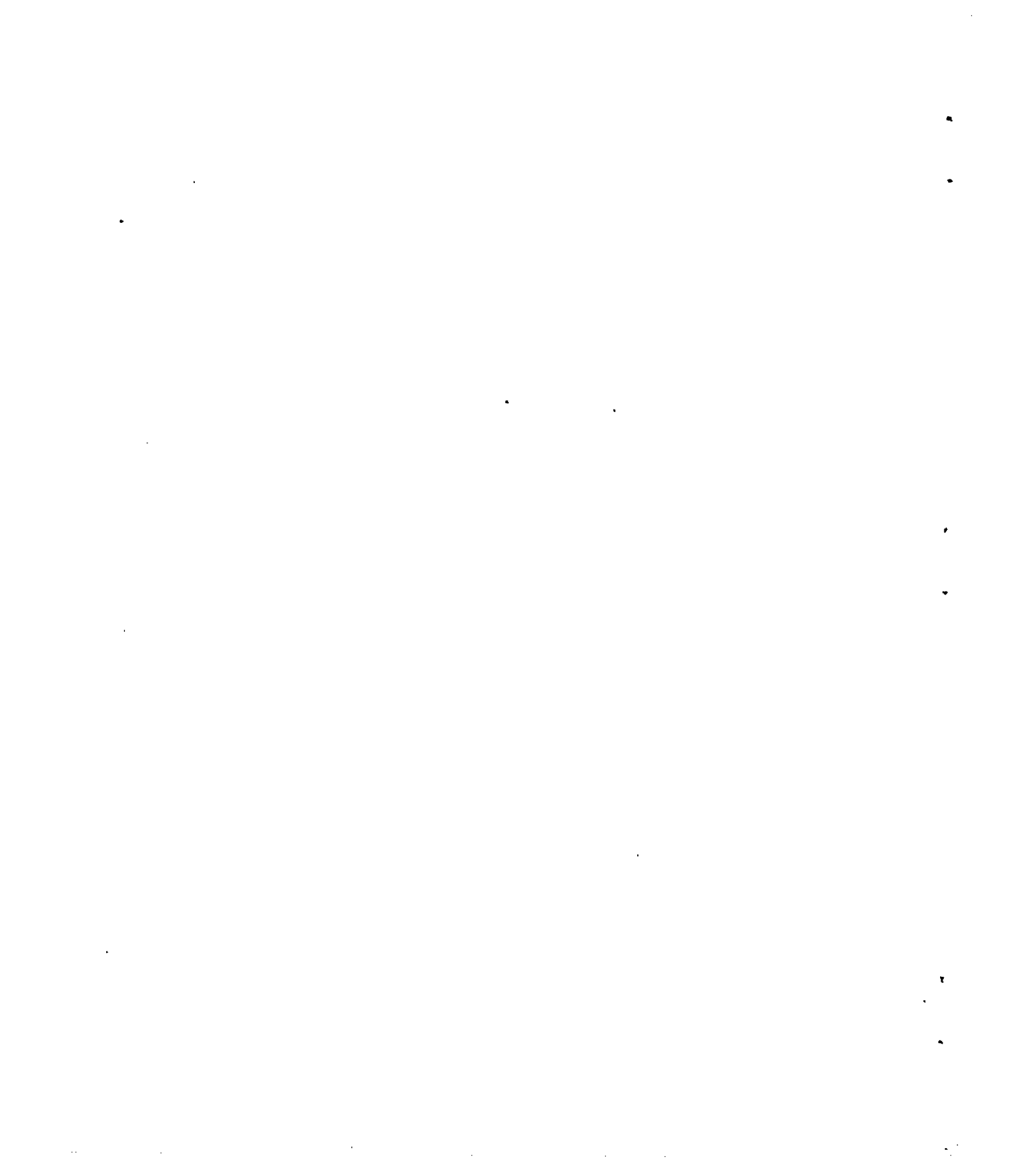
Figure 2.— Models as mounted for investigation in Ames 40- by 80-foot wind tunnel.





(b) Modified-wedge wing-body model.

Figure 2.- Continued.



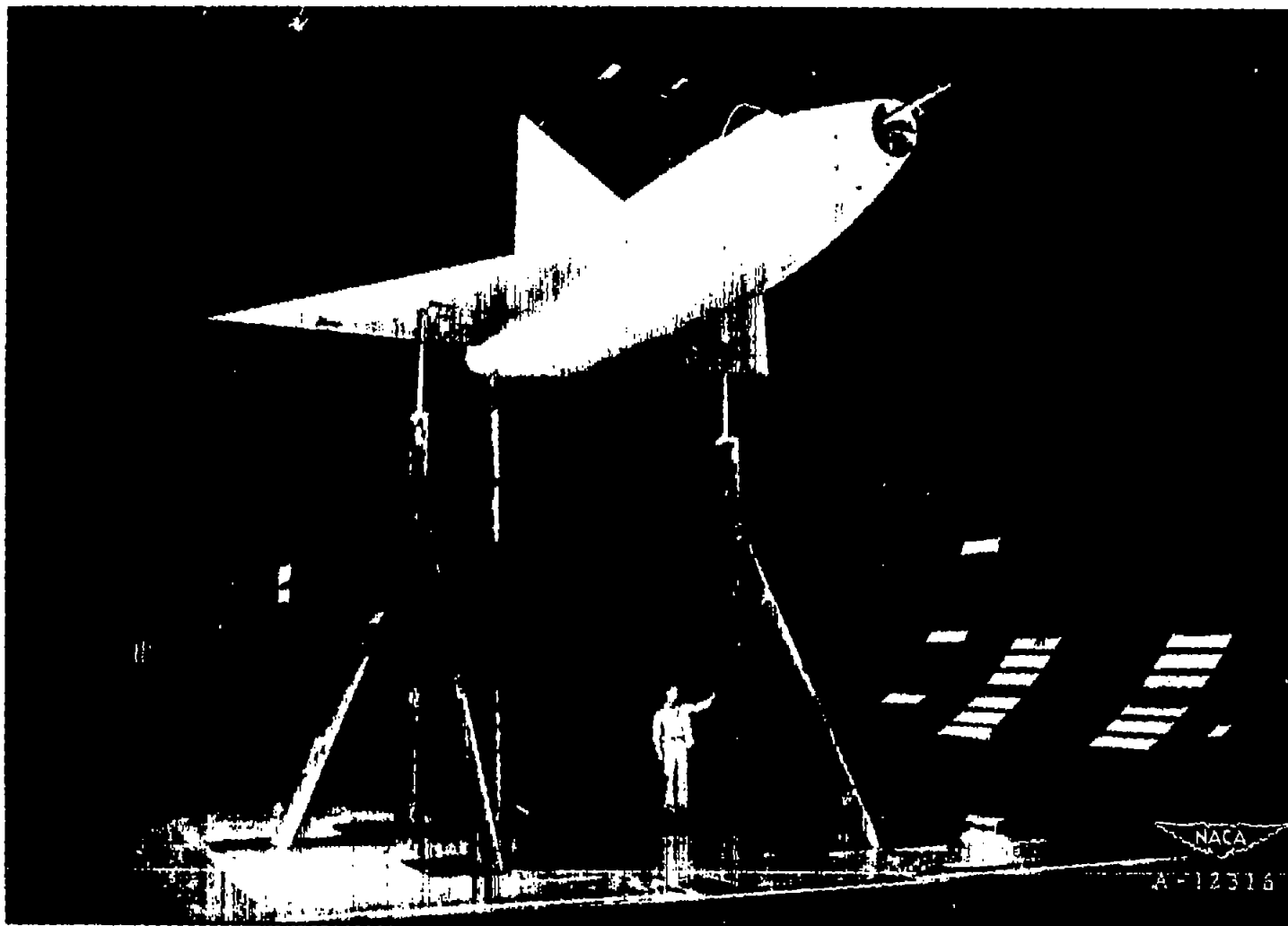
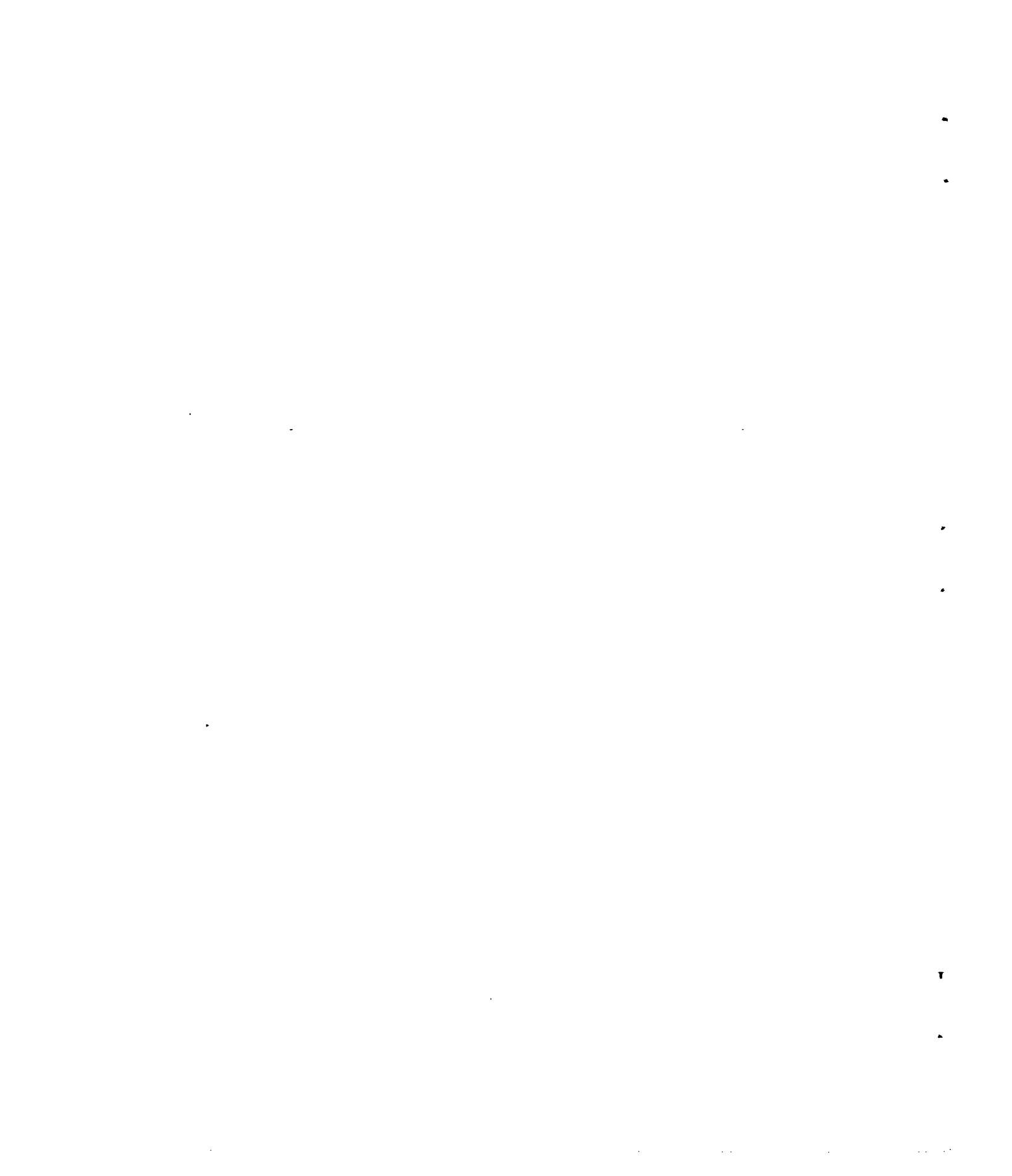
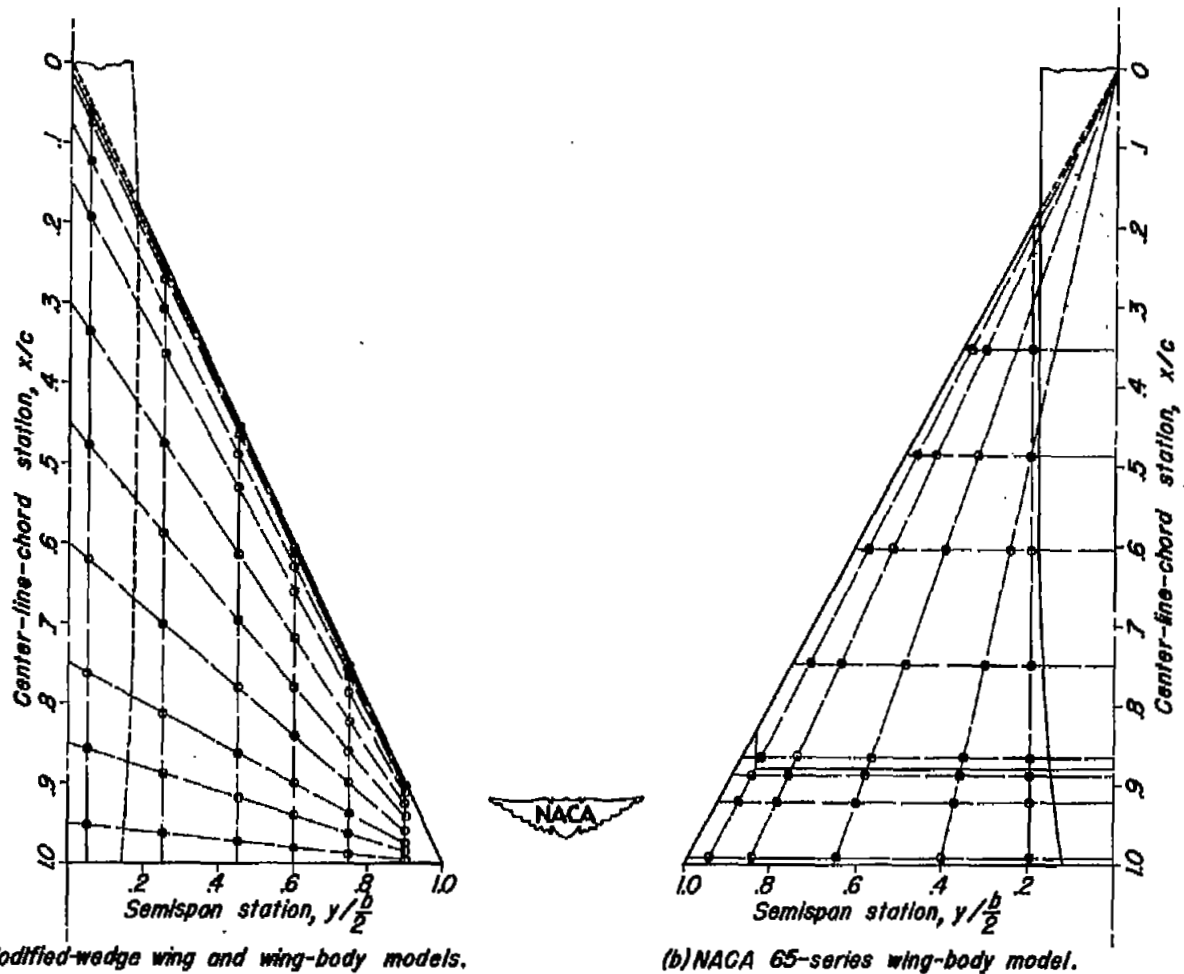


Figure 2.- Concluded.

(c) NACA 65-series wing-body model.





(a) Modified-wedge wing and wing-body models.
 (b) NACA 65-series wing-body model.
 Figure 3.- Approximate pressure orifice distribution.

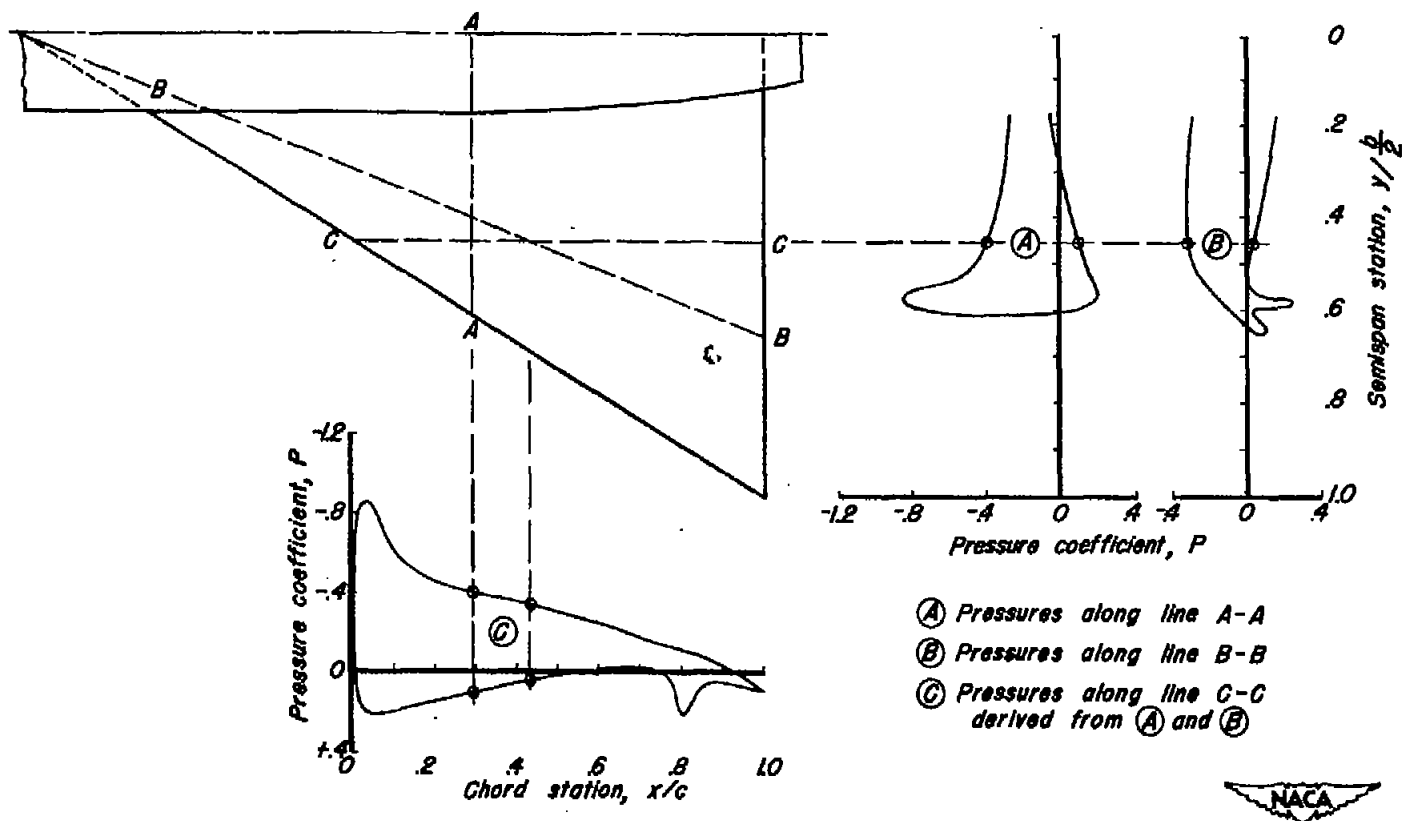


Figure 4.- Method of deriving chordwise pressure diagrams on NACA 65-series wing-body model.

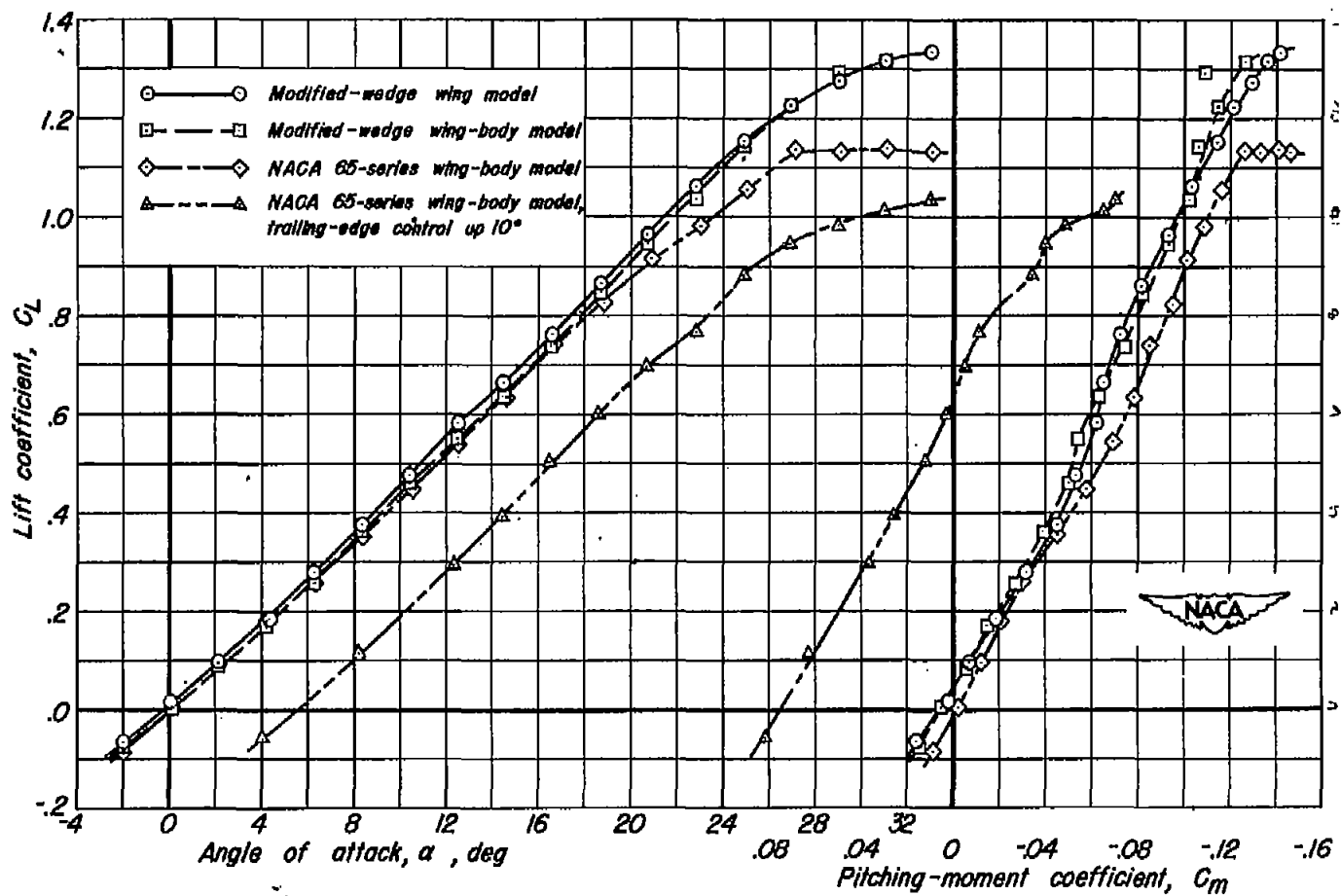
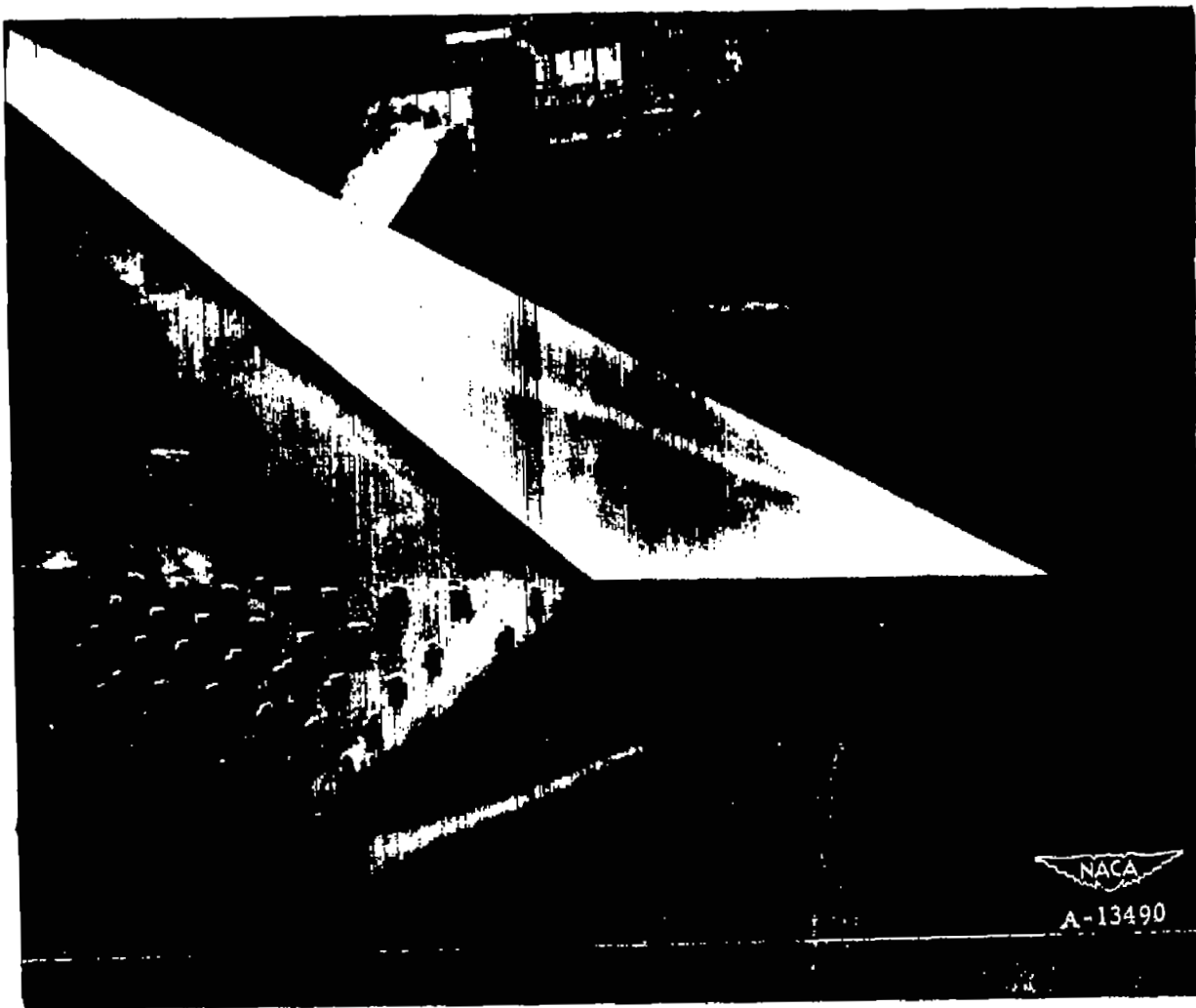
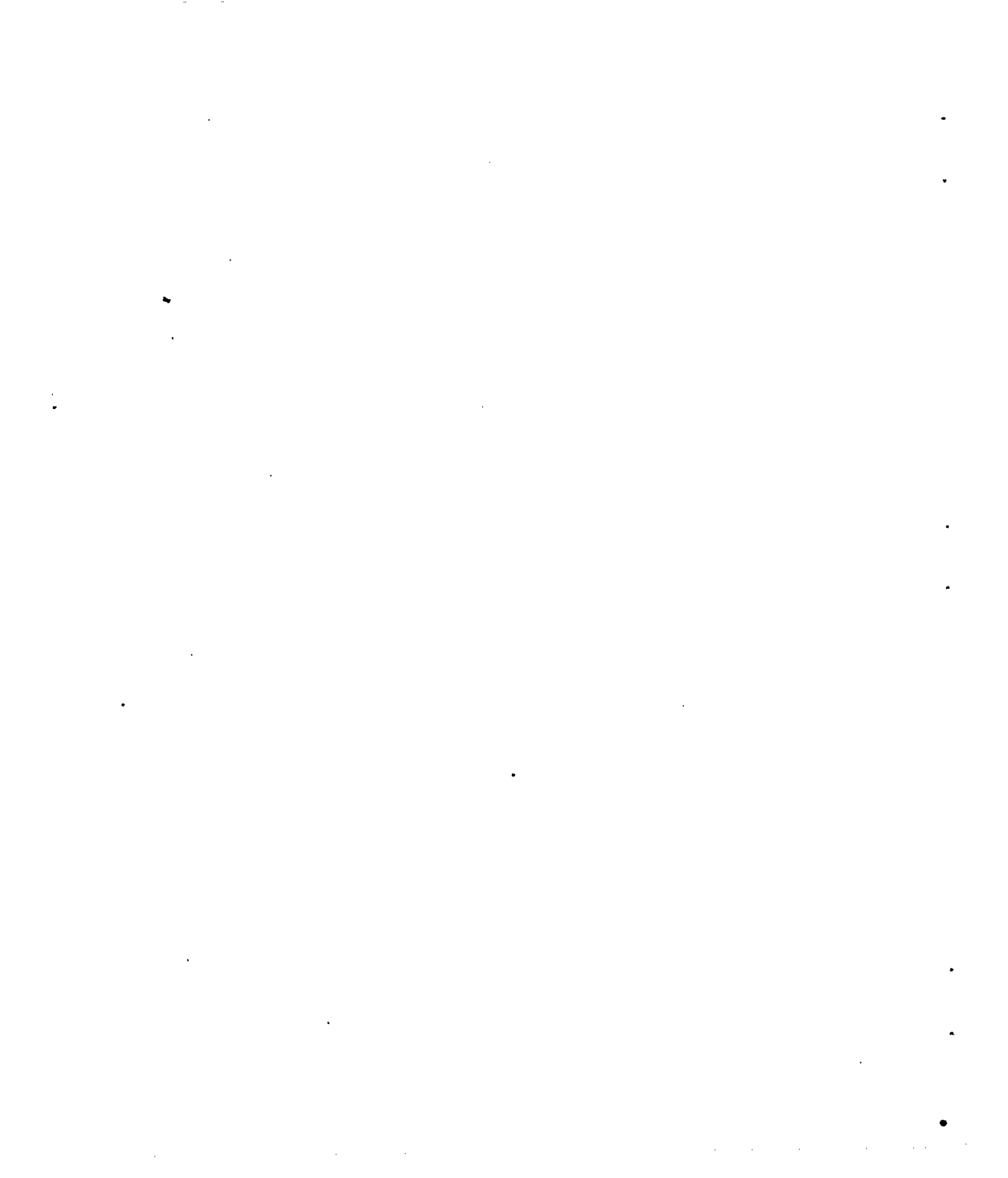


Figure 5.- Force test lift and pitching-moment curves.





(a) Photograph of vortices on double-wedge section triangular wing; α , 24.9° .
 Figure 6.- Separation vortices on triangular plan-form wings.



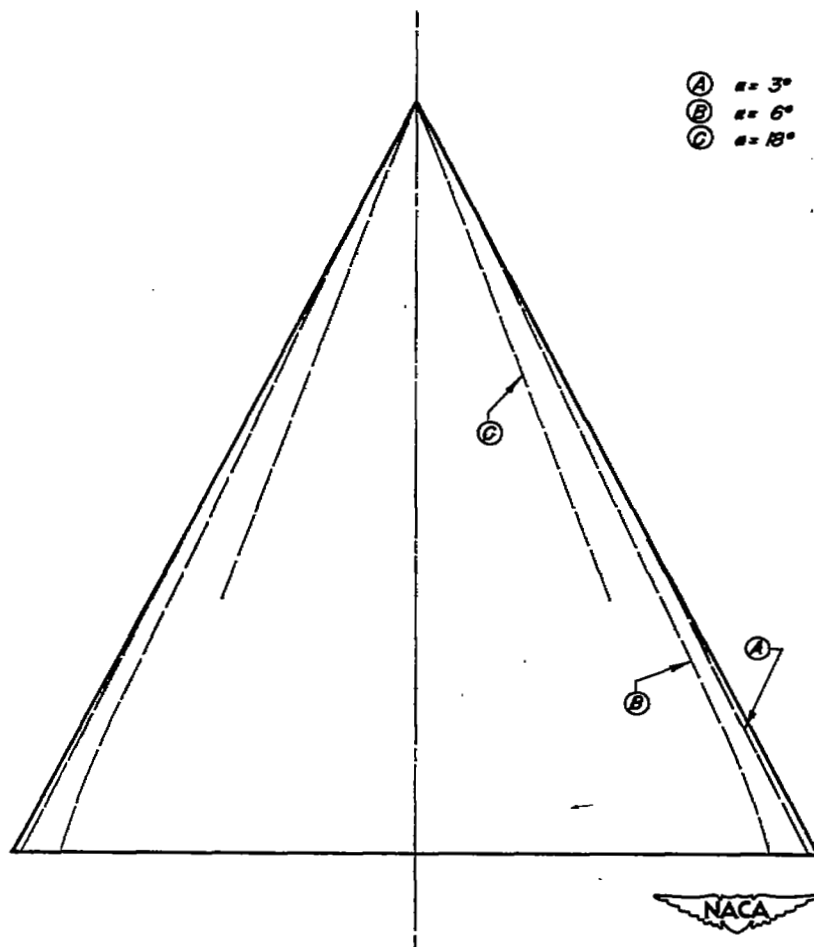
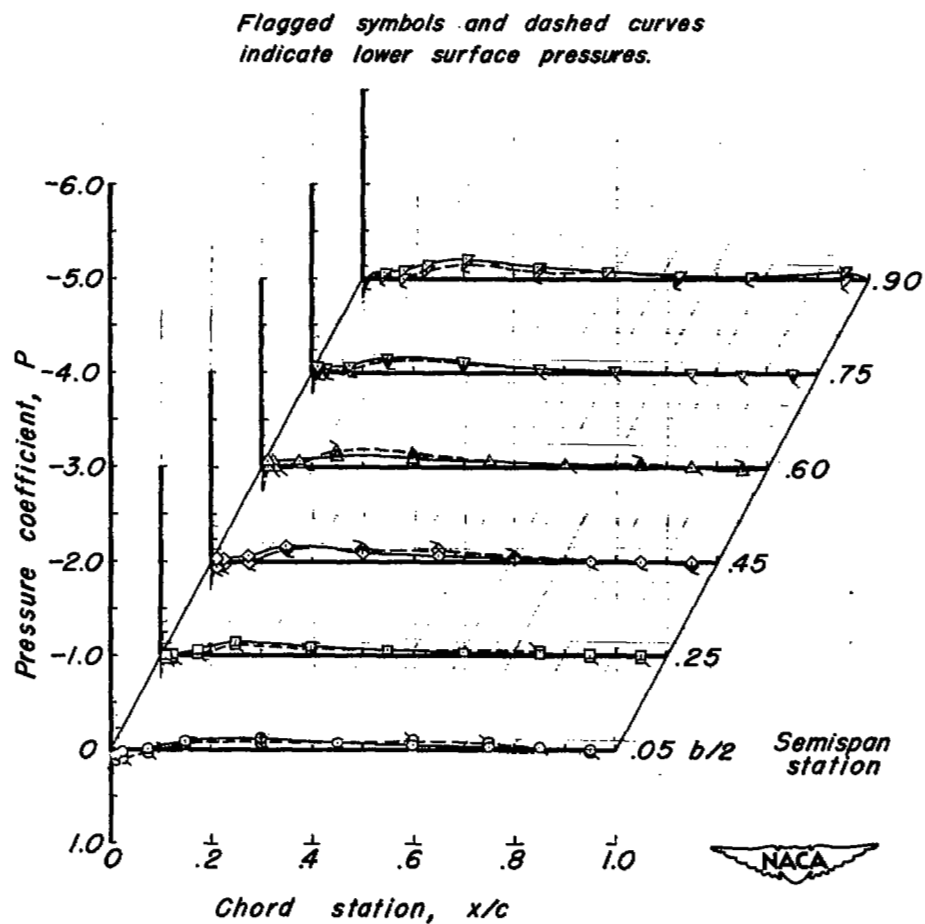
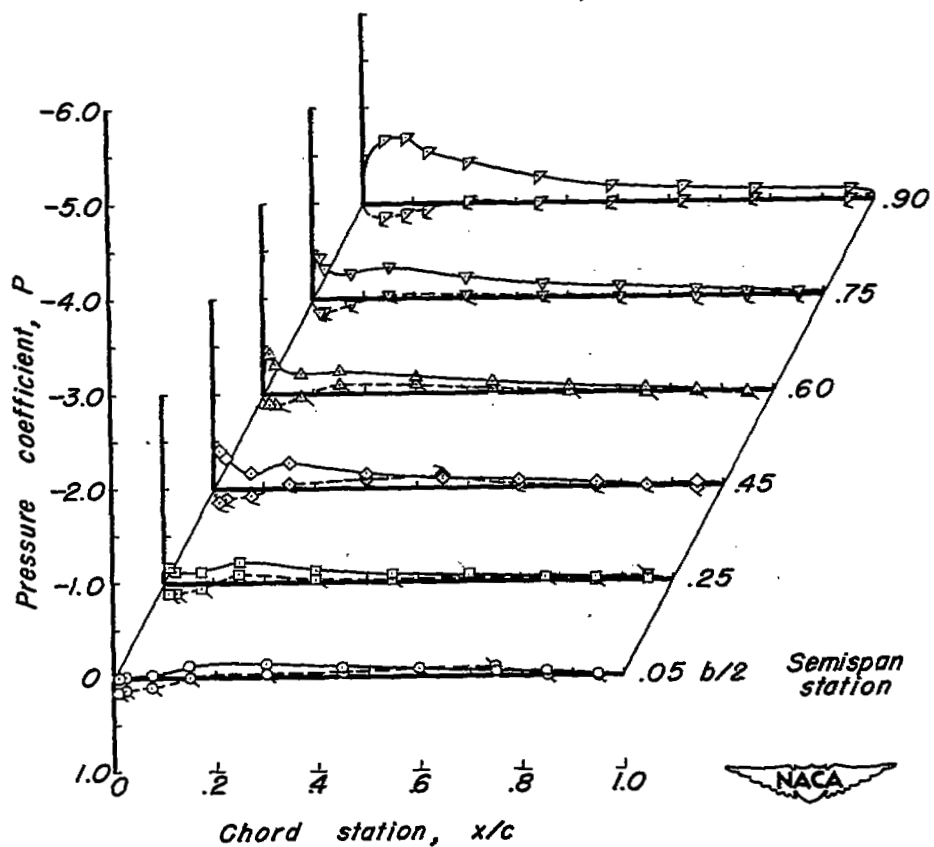


Figure 6.- Concluded.



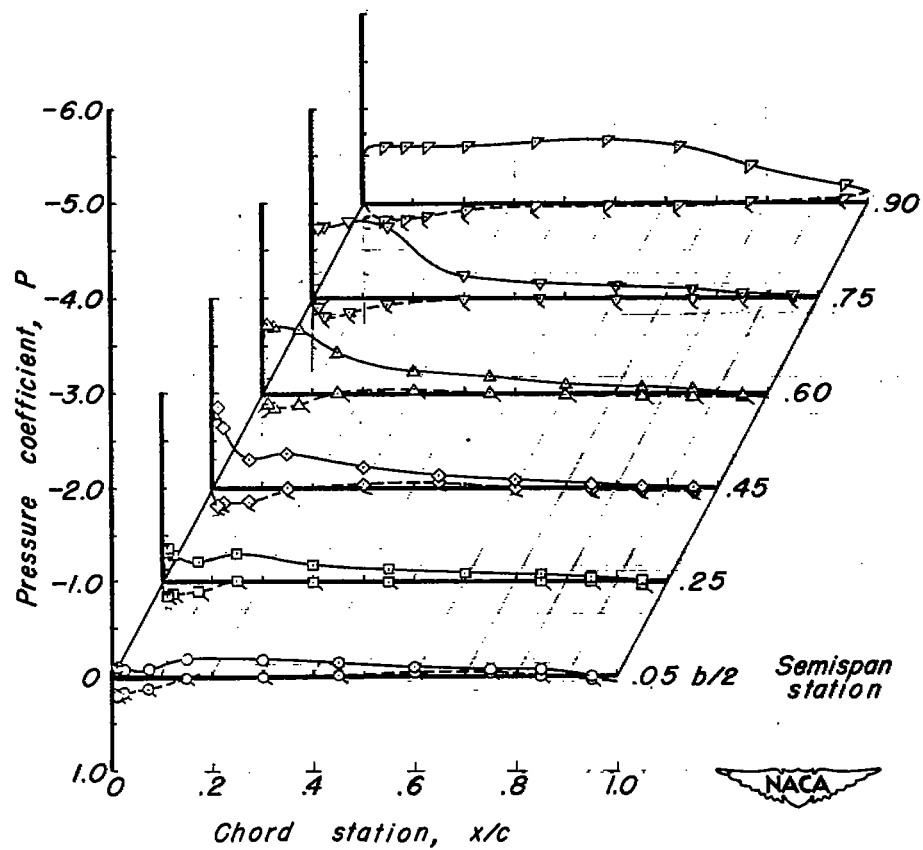
(a) $\alpha, 0.0^\circ$.

Figure 7.- Pressure distribution along chord for various angles of attack of modified-wedge wing model.



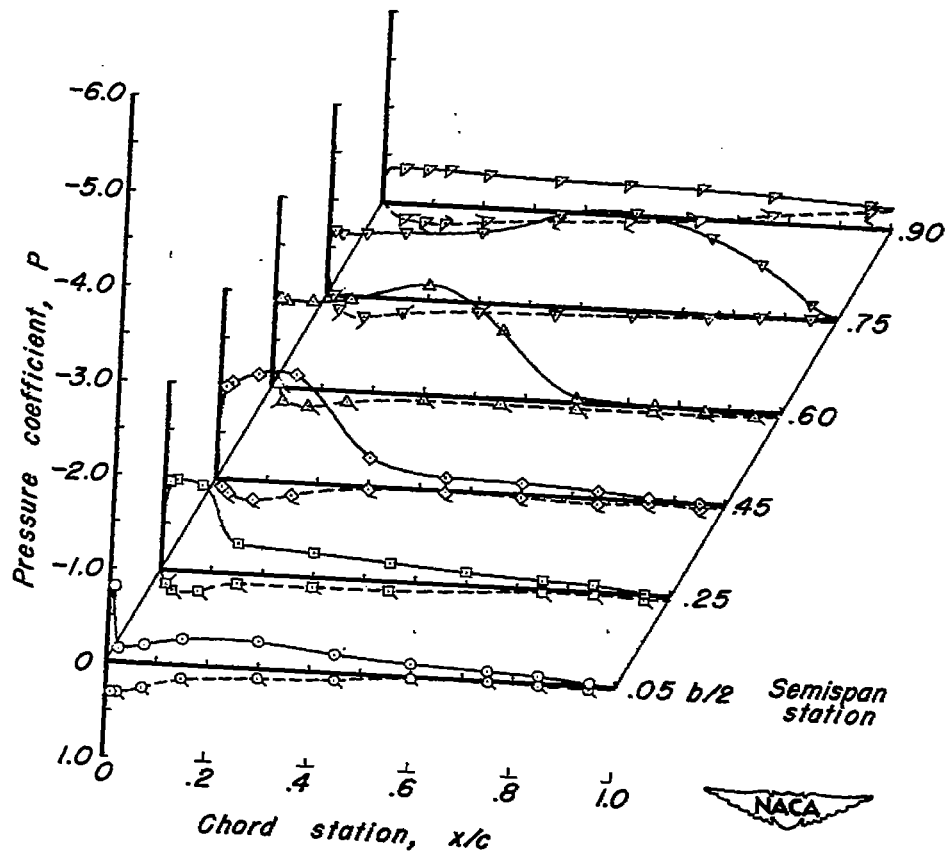
(b) $\alpha, 2.1^\circ$.

Figure 7.- Continued.



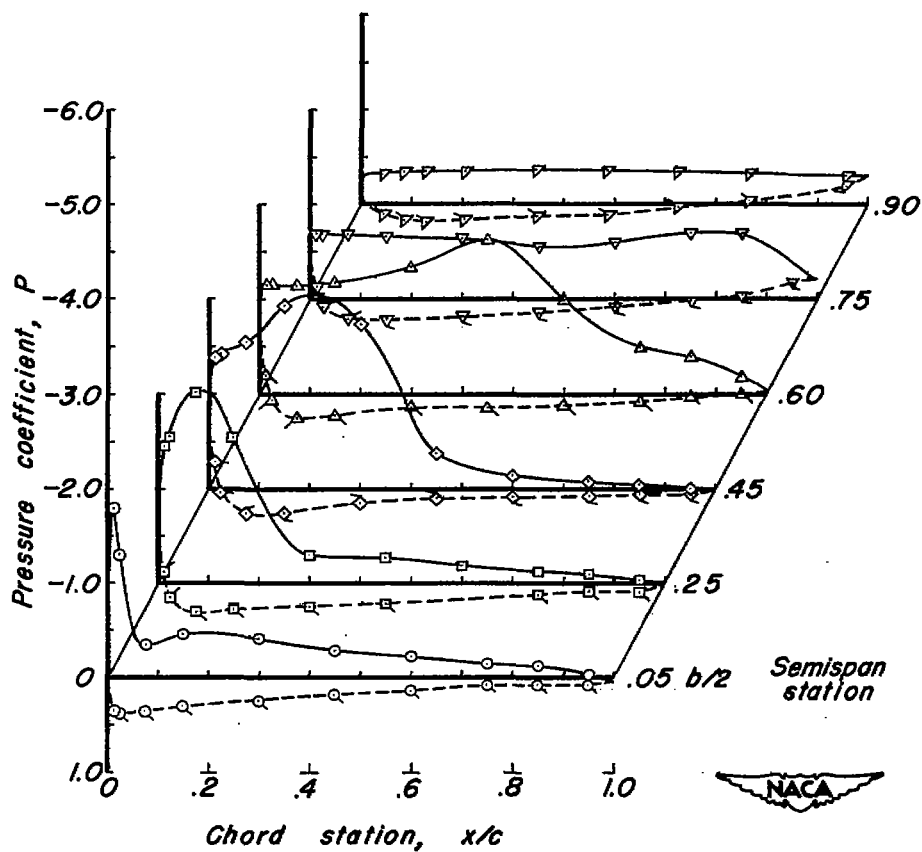
(c) α , 4.2° .

Figure 7.- Continued.



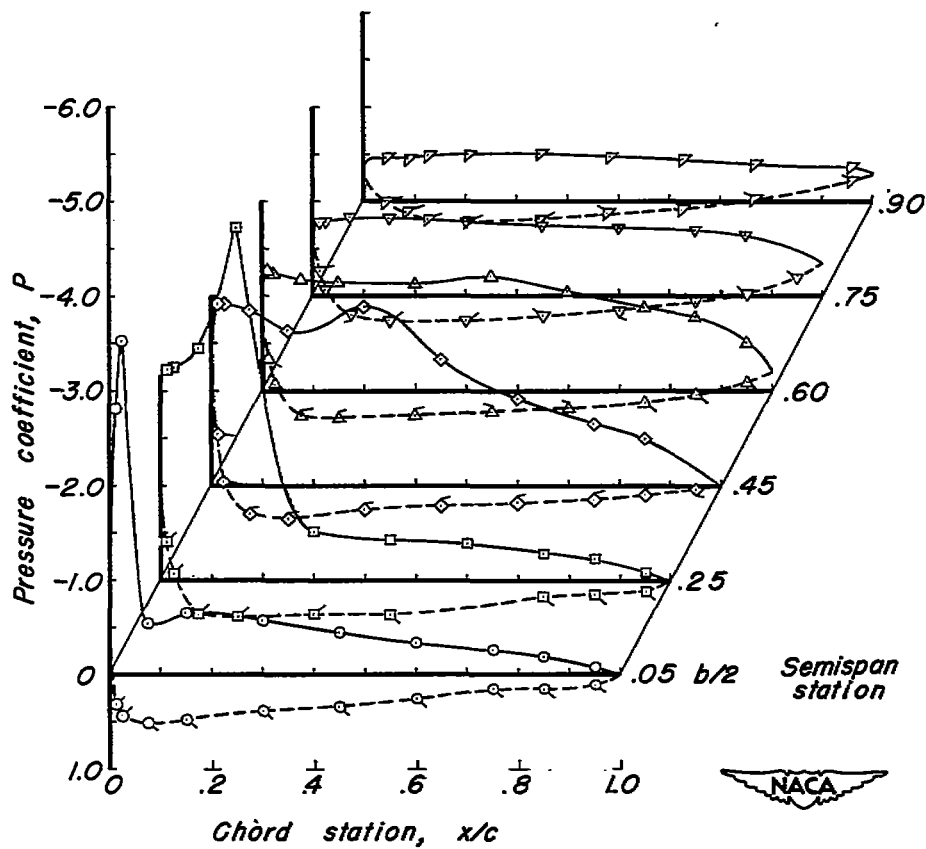
(d) $\alpha, 8.3^\circ$.

Figure 7.- Continued.



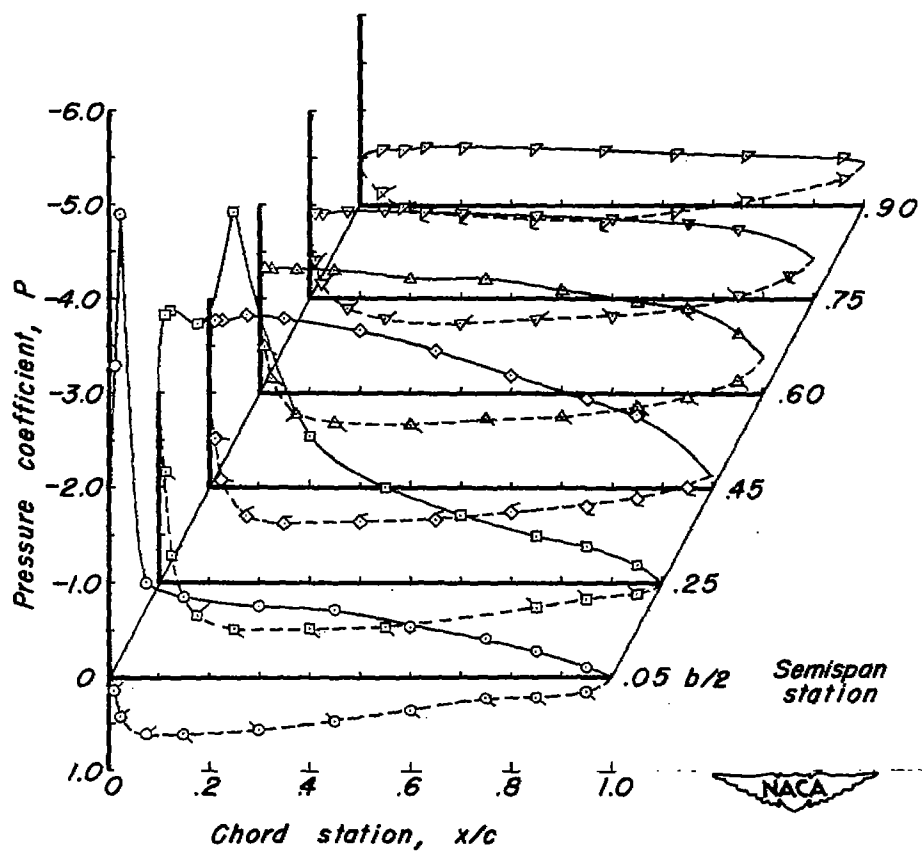
(e) $\alpha, 14.5^\circ$.

Figure 7.- Continued.



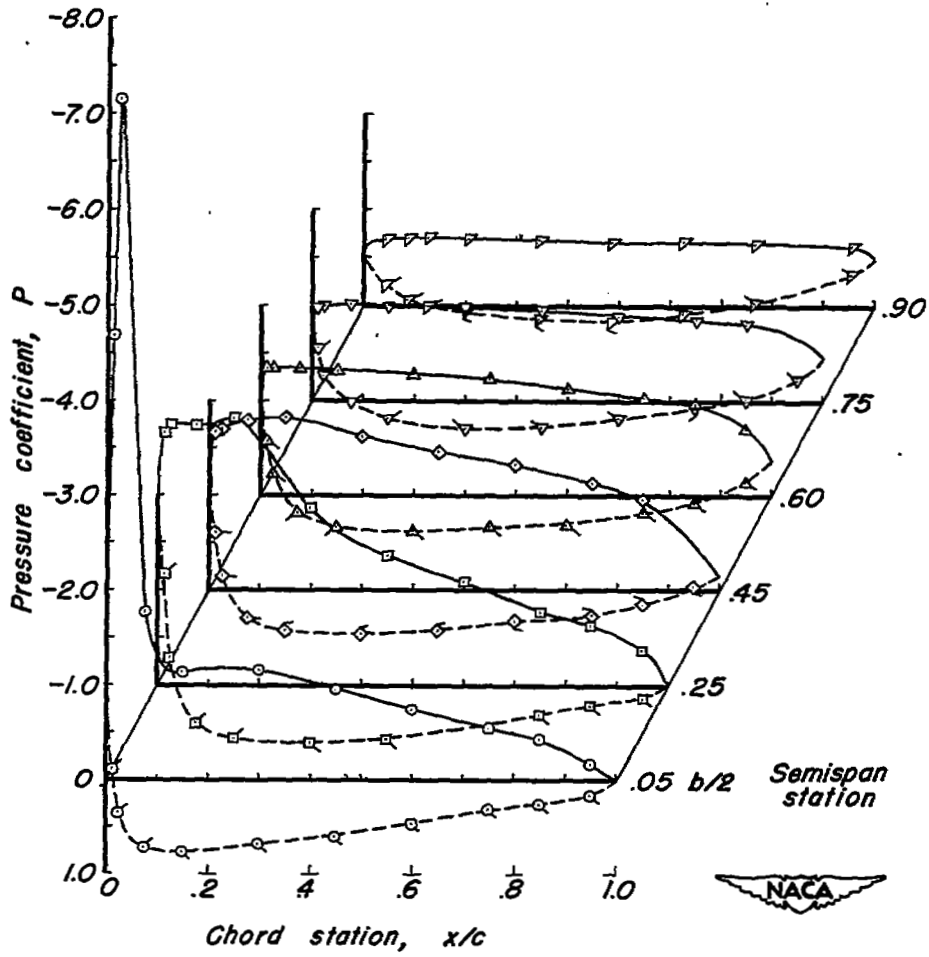
(f) $\alpha, 20.8^\circ$.

Figure 7.- Continued.



(g) α , 26.9° .

Figure 7.- Continued.



(h) $\alpha, 33.0^\circ$.

Figure 7.- Concluded.



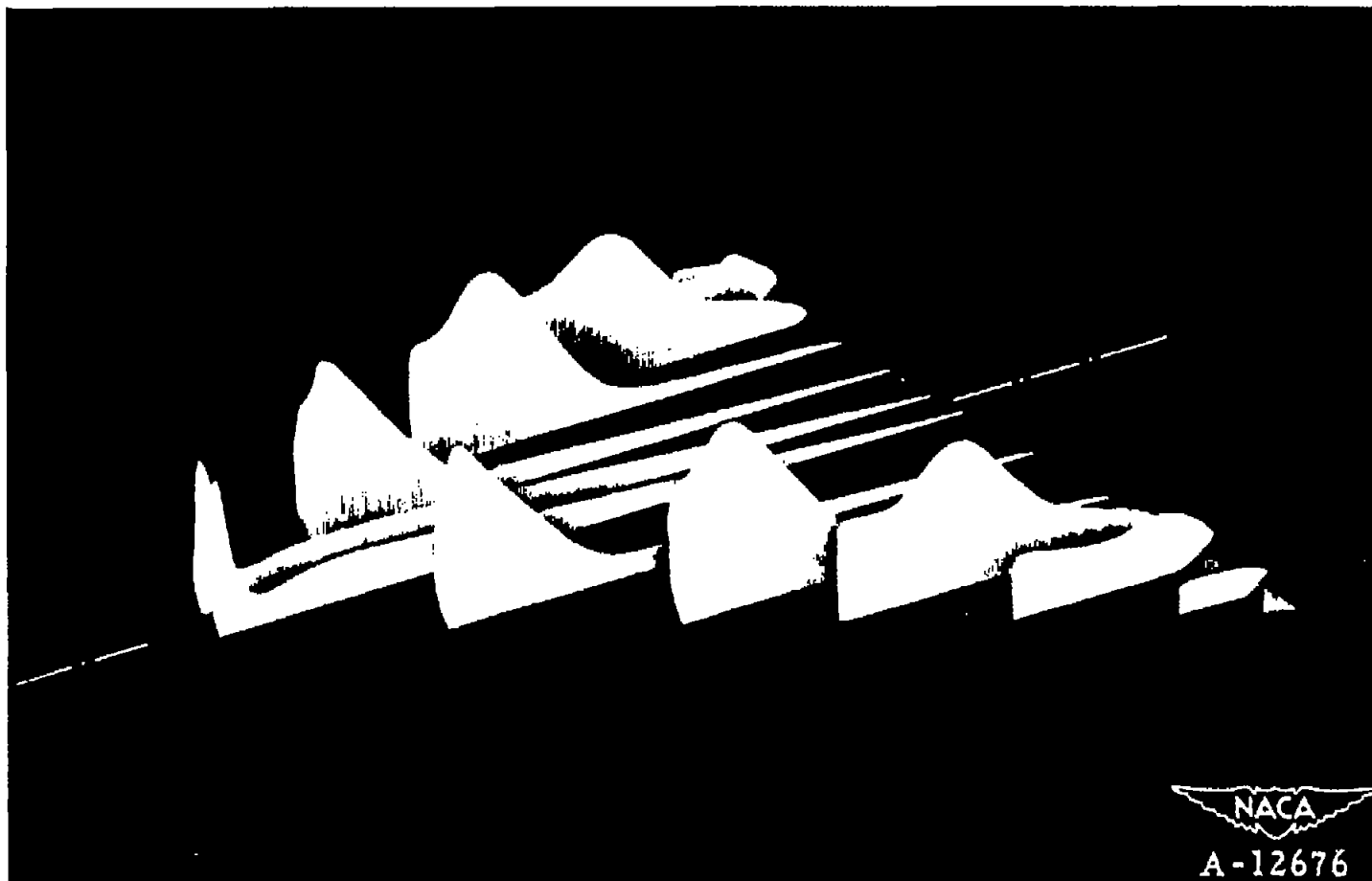
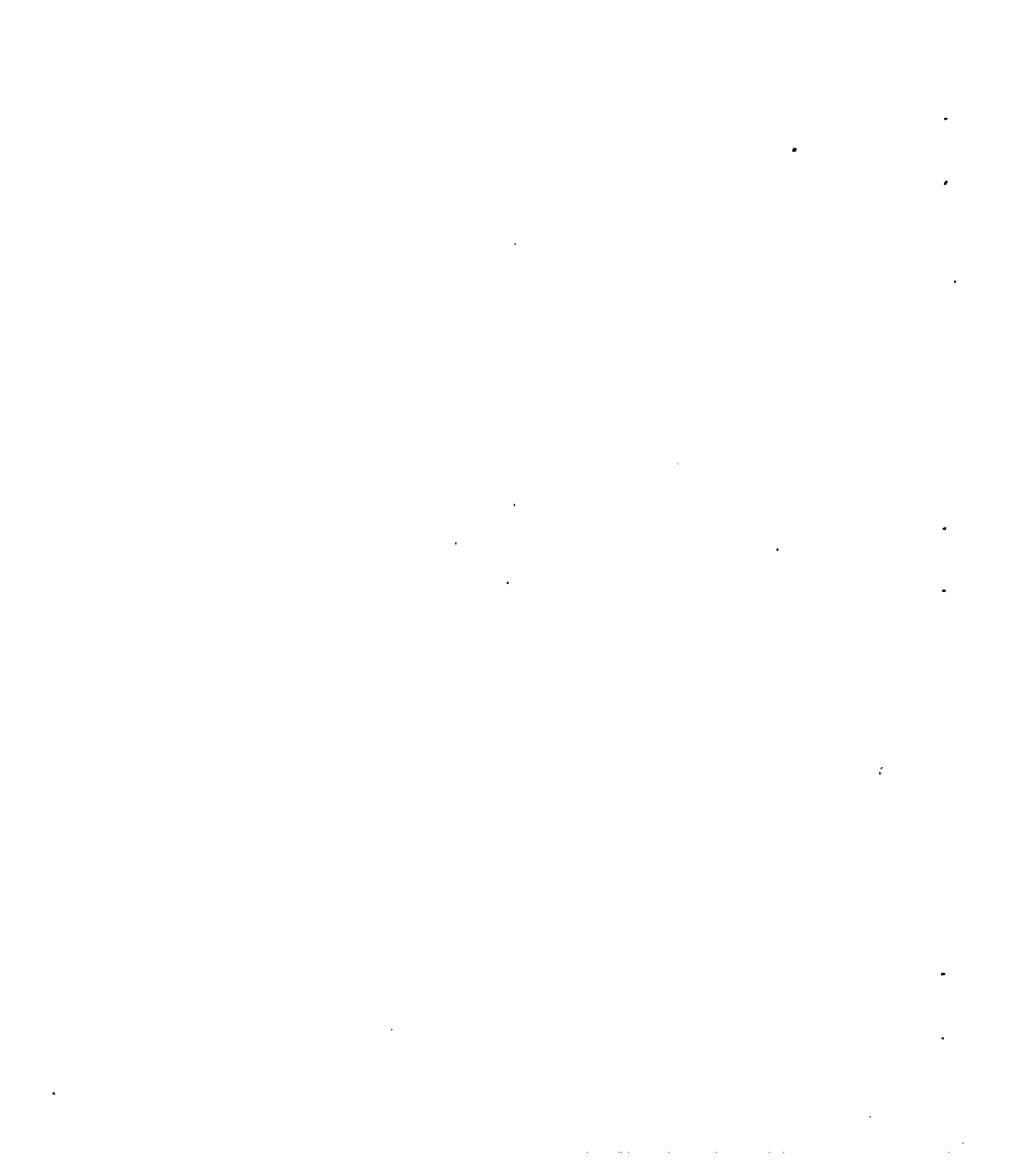
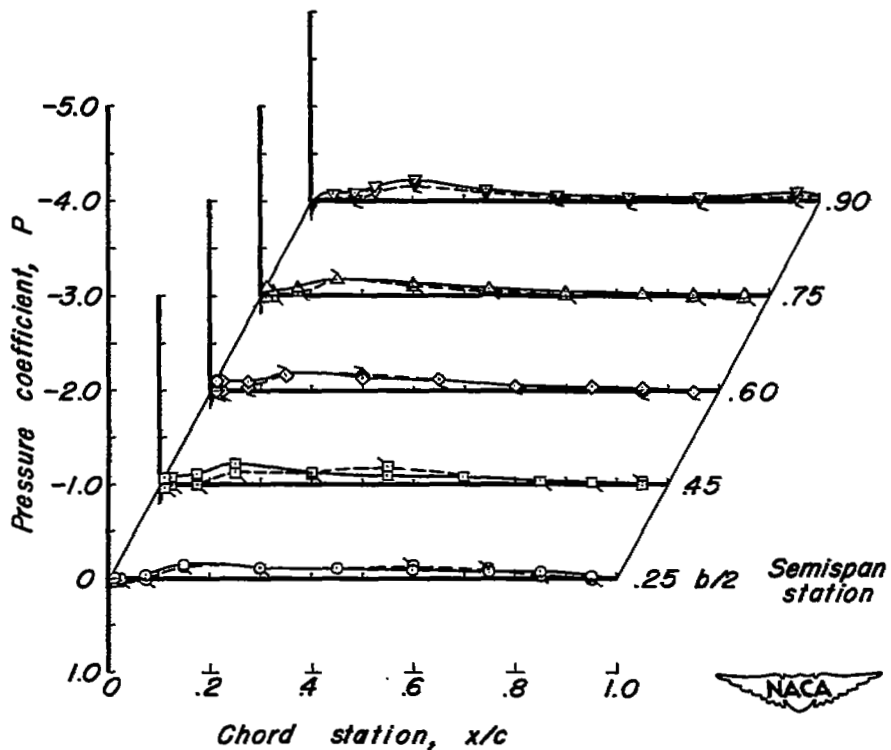


Figure 8.- Pressures on top surface of the modified-wedge wing model; α , 14.5° .

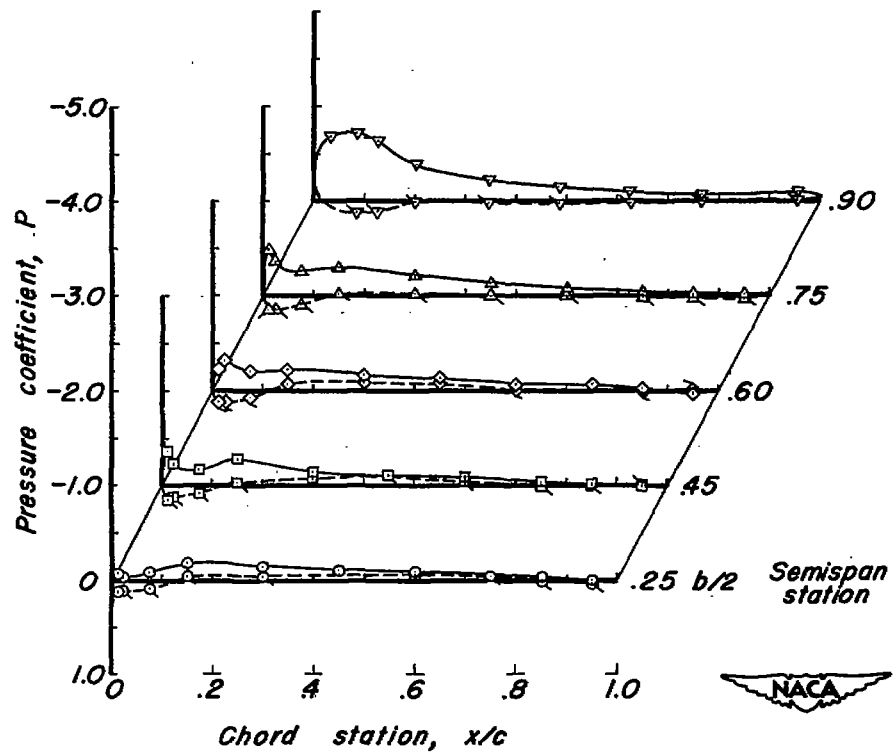


Flagged symbols and dashed curves indicate lower surface pressures.



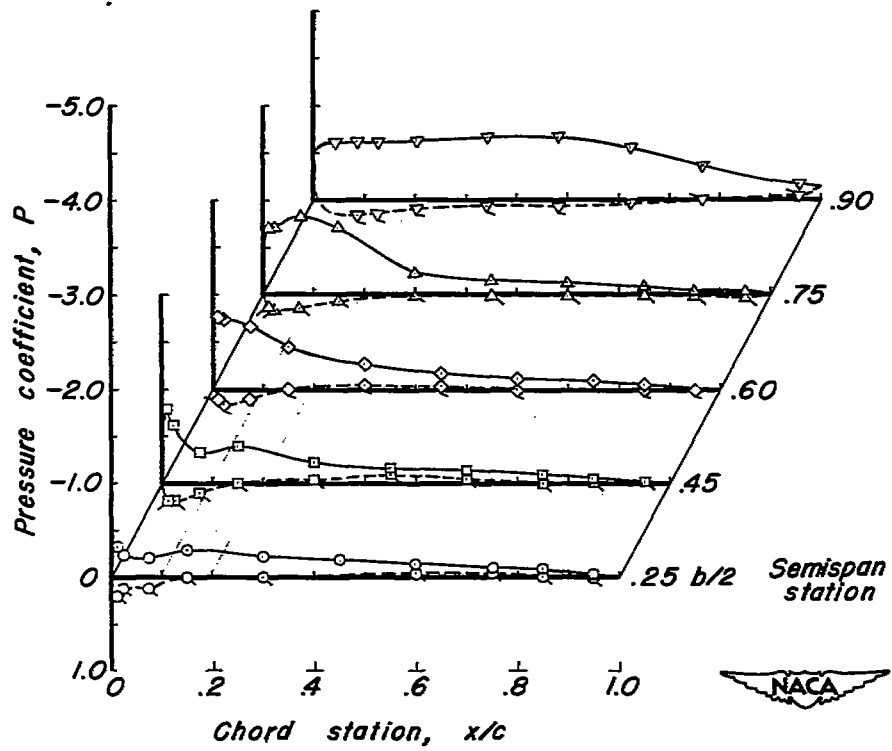
(a) $\alpha, 0.0^\circ$

Figure 9.- Pressure distribution along chord for various angles of attack of modified-wedge wing-body model.



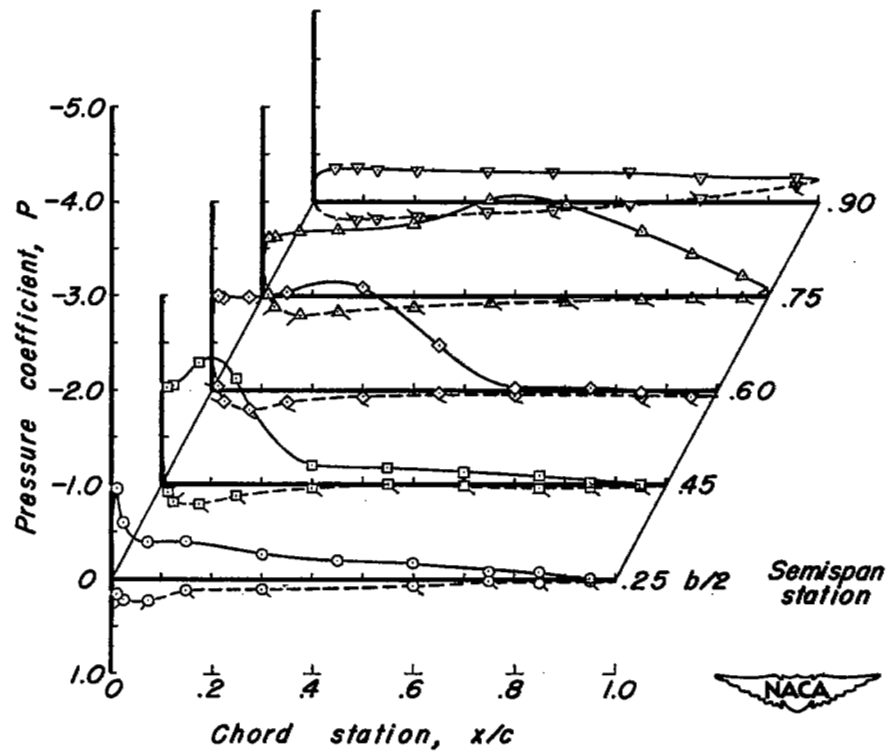
(b) α , 2.1° .

Figure 9.- Continued.



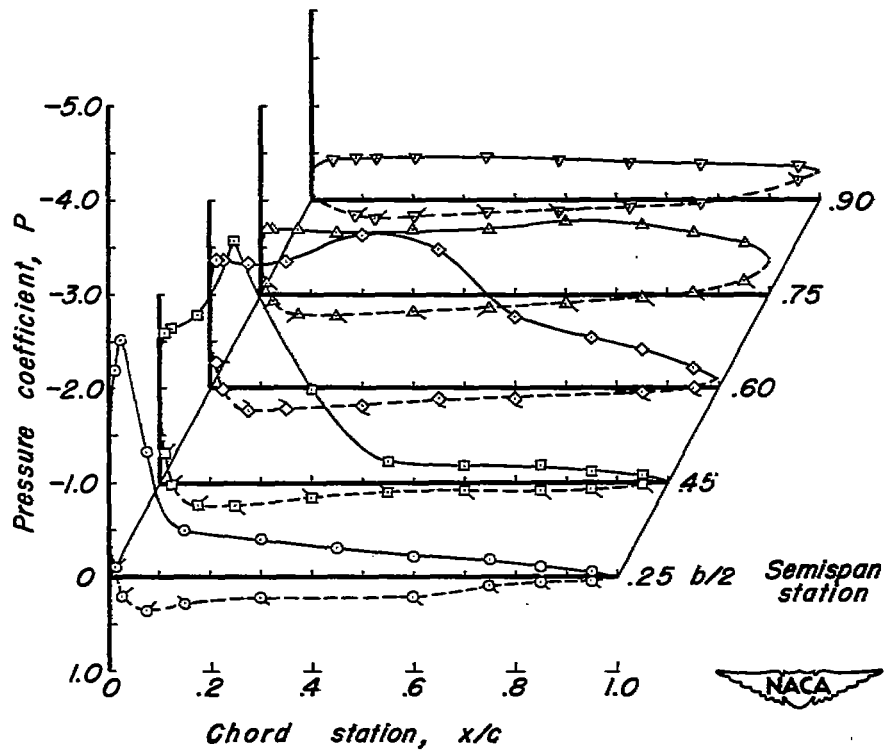
(c) $\alpha, 4.2^\circ$.

Figure 9.- Continued.



(d) α , 8.3° .

Figure 9.- Continued.



(e) α , 14.5°

Figure 9.- Continued.

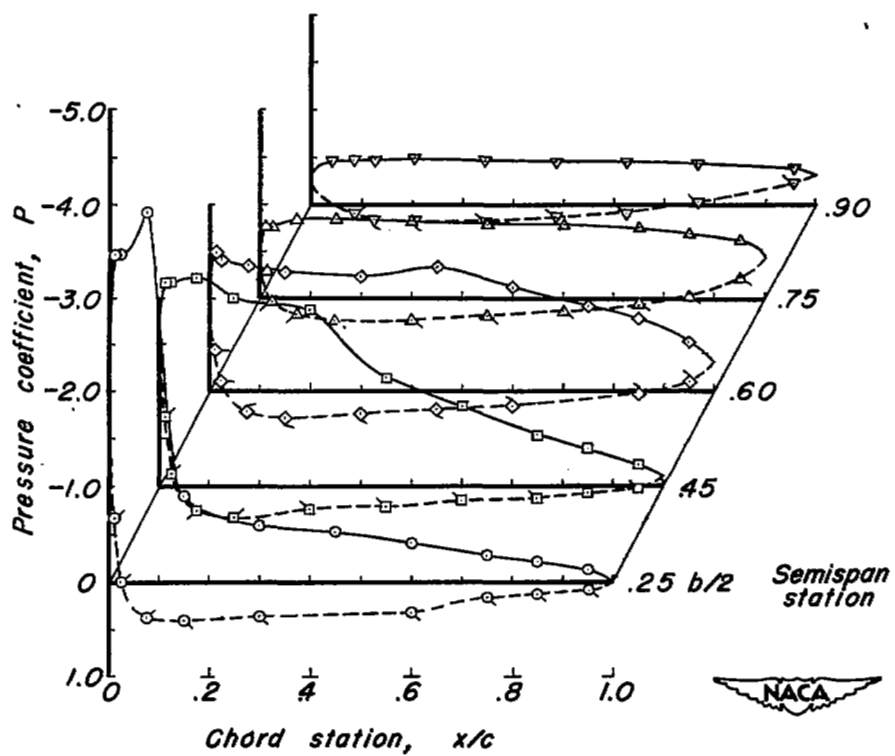
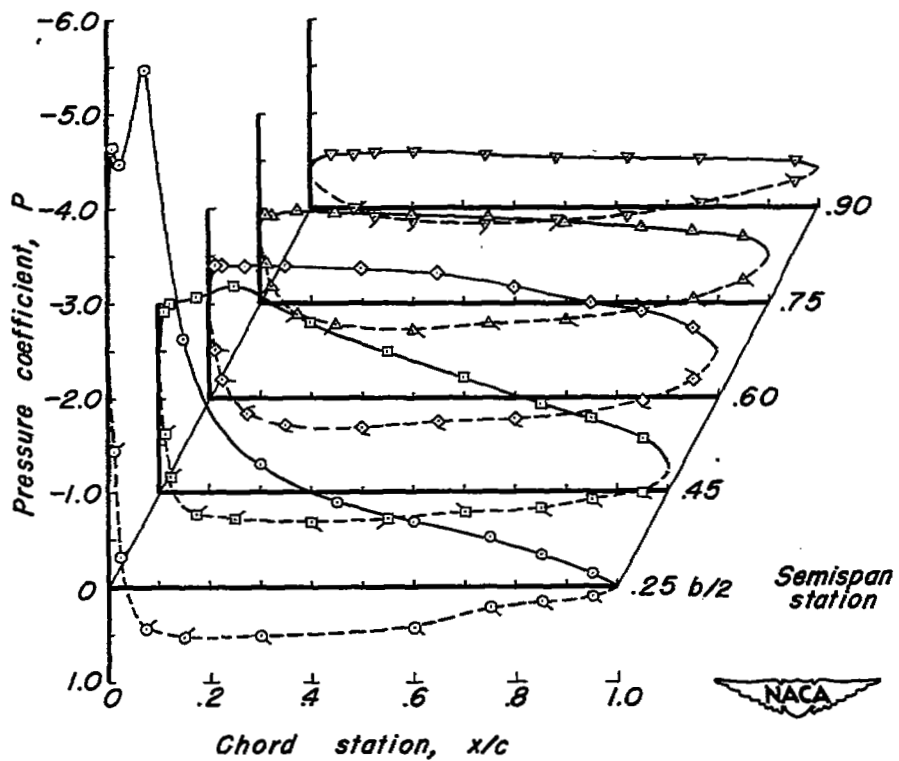
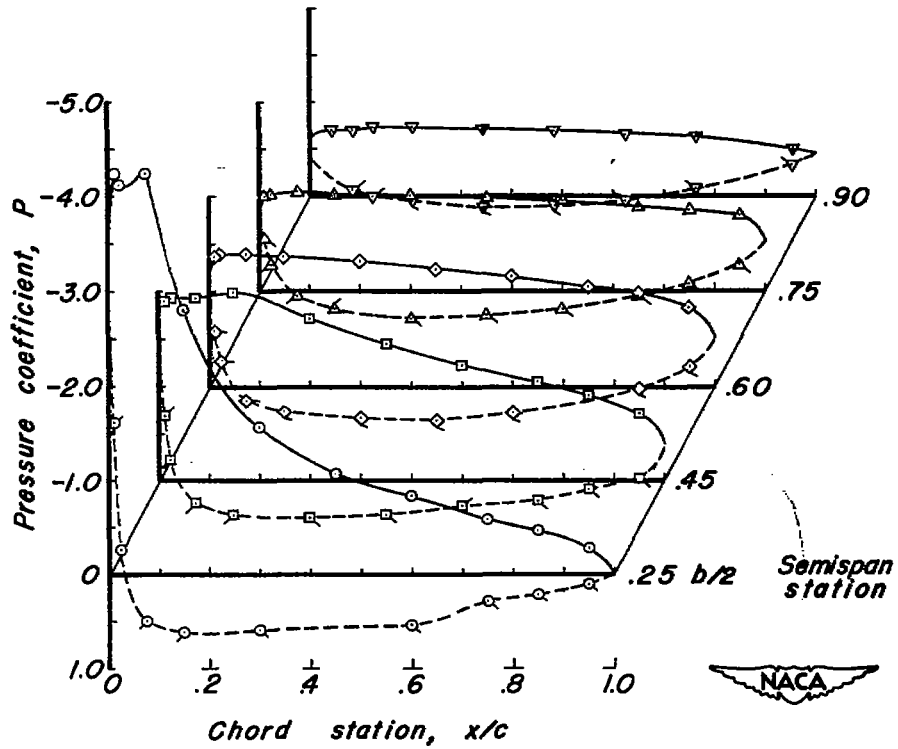
(f) α , 20.7° .

Figure 9.- Continued.



(g) α , 26.9° .

Figure 9.- Continued.



(h) α , 31.0° .

Figure 9.— Concluded.

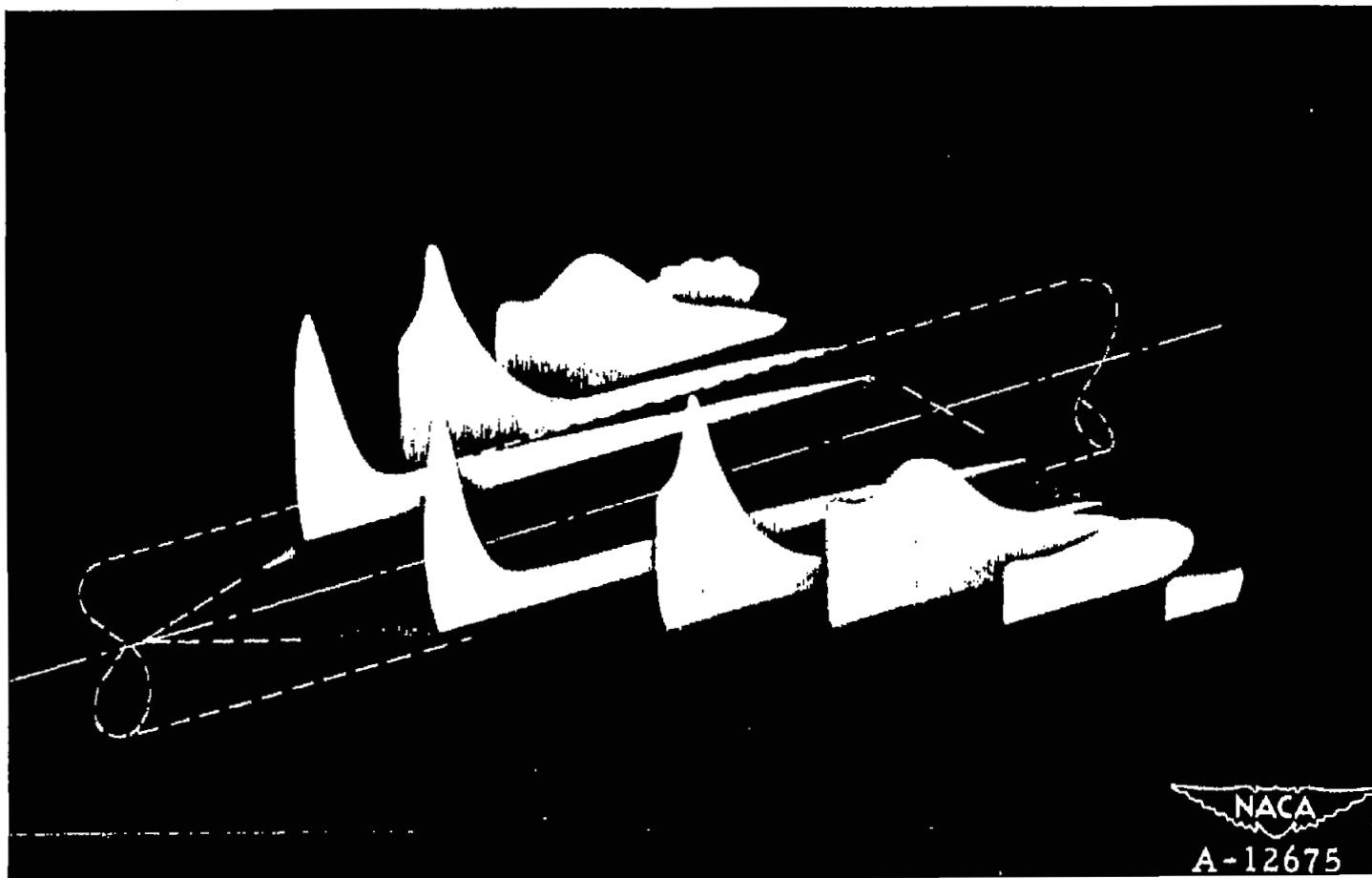
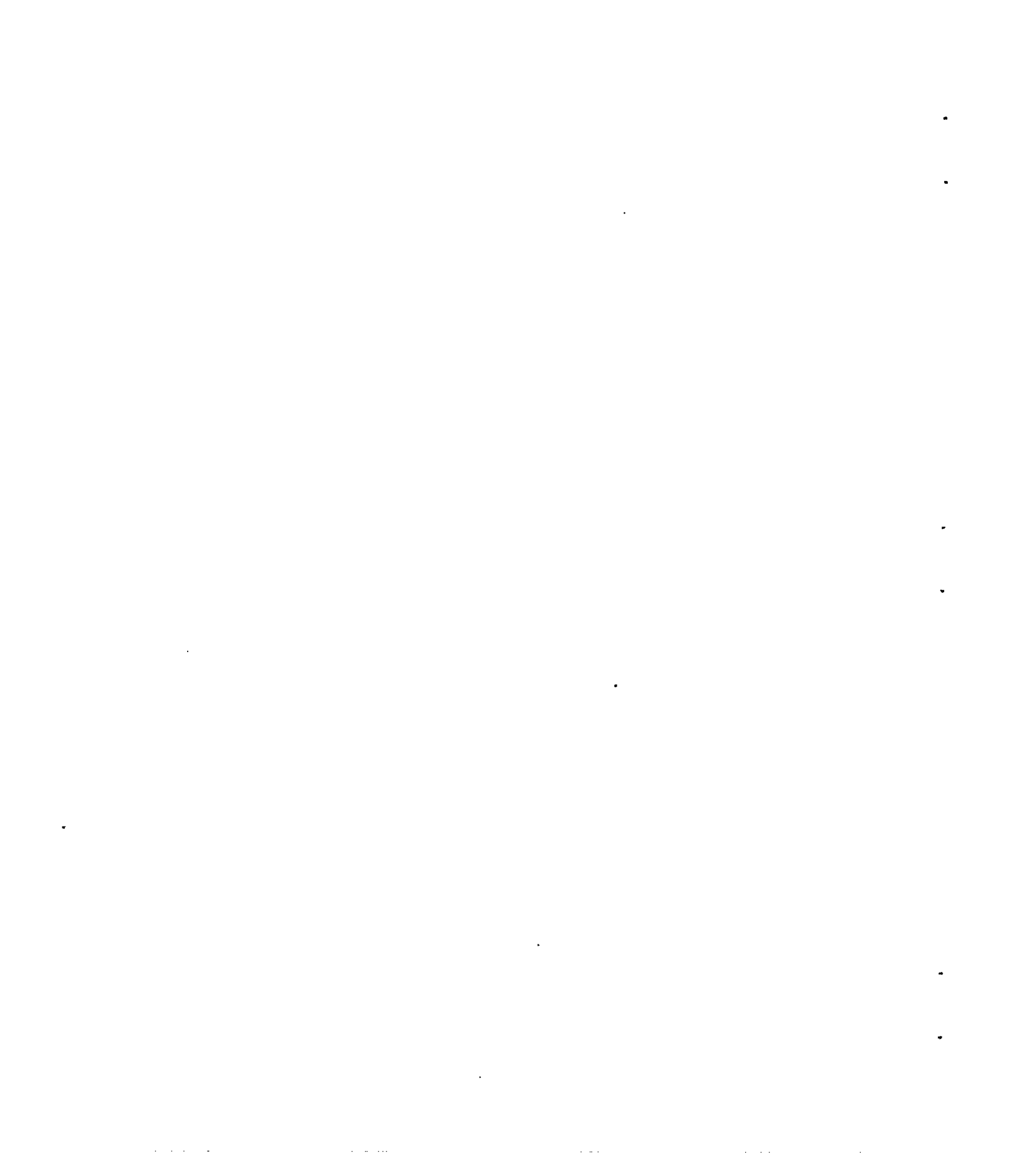
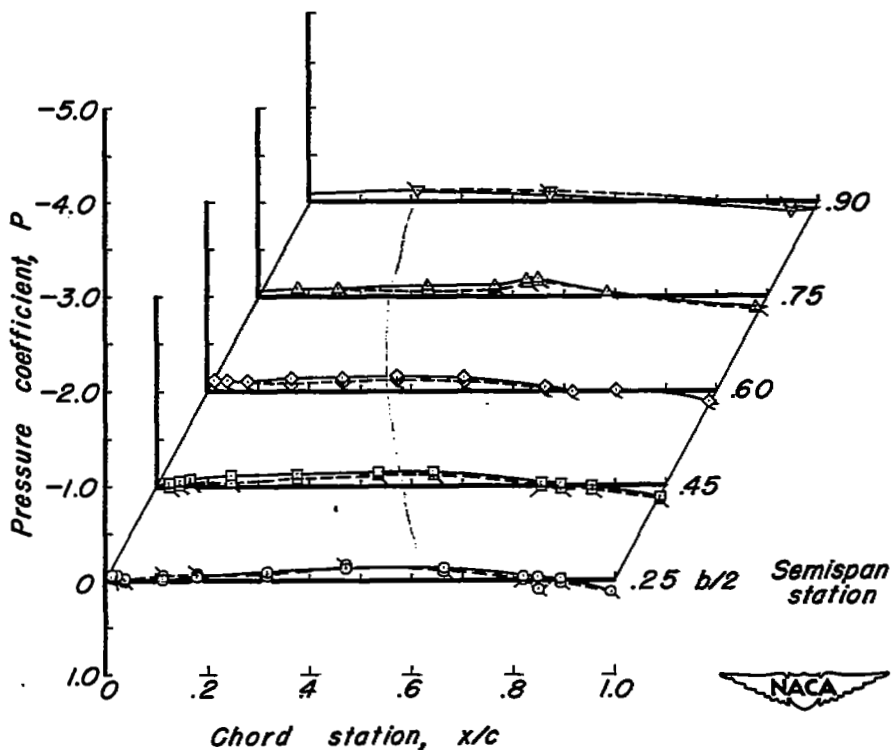


Figure 10.- Pressures on top surface of modified-wedge wing body model; α , 14.5° .

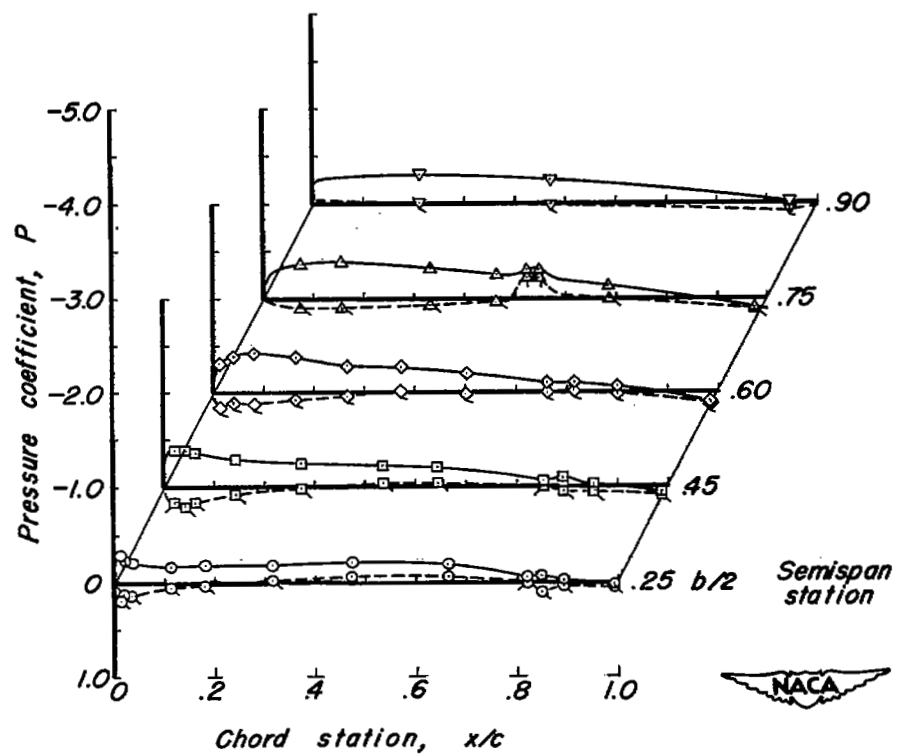


Flagged symbols and dashed curves indicate lower surface pressures.



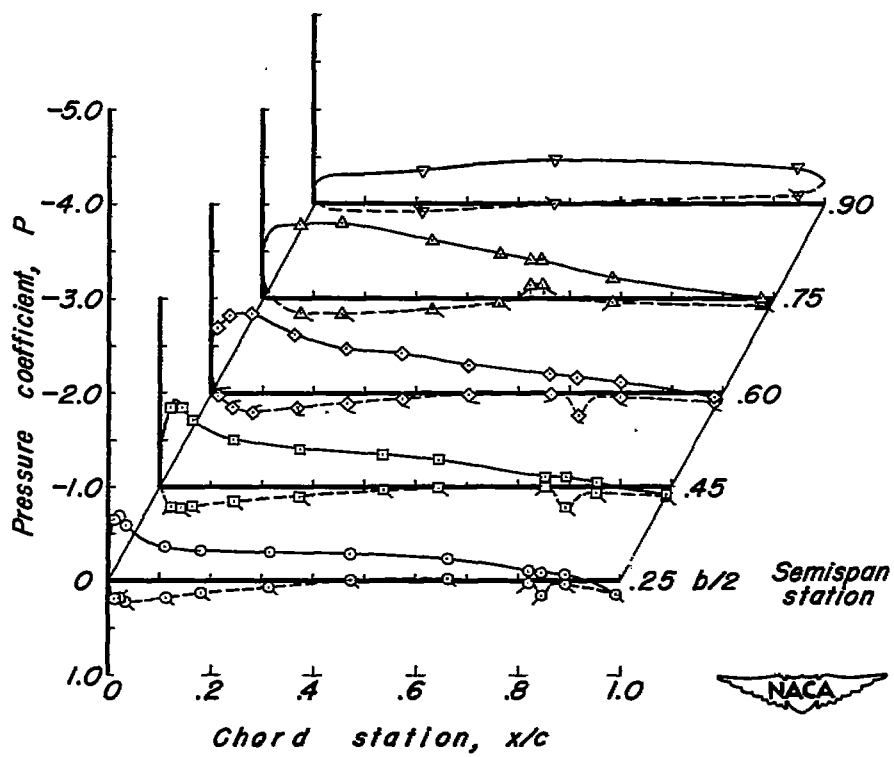
(a) α , 0.1° .

Figure 11.- Pressure distribution along chord for various angles of attack of NACA 65-series wing-body model controls neutral.



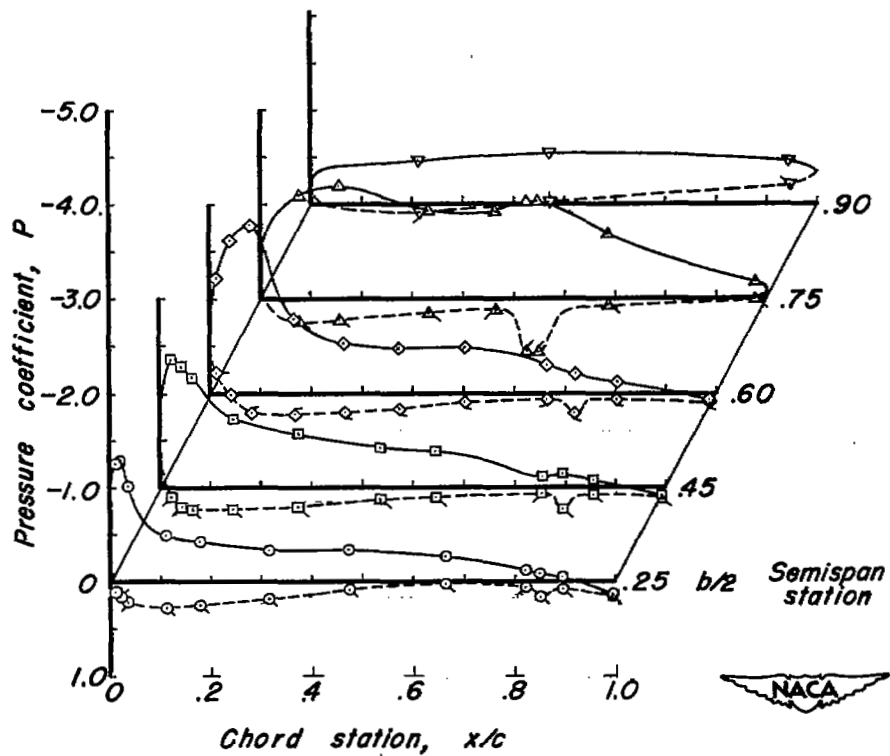
(b) α , 4.2° .

Figure 11.- Continued.



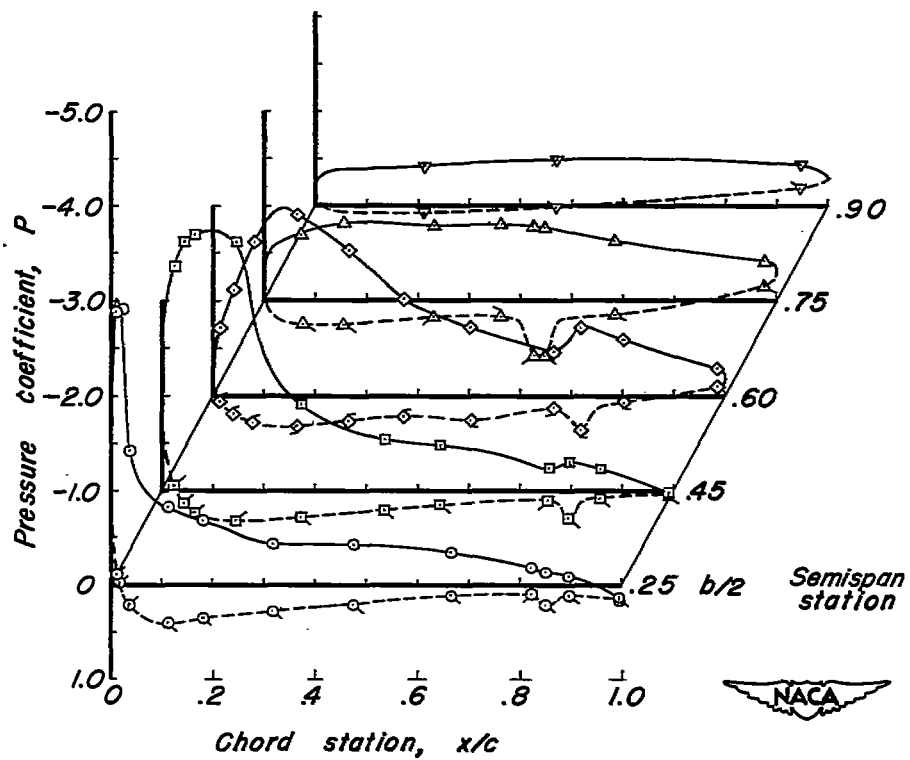
(c) α , 8.3°.

Figure 11.- Continued.



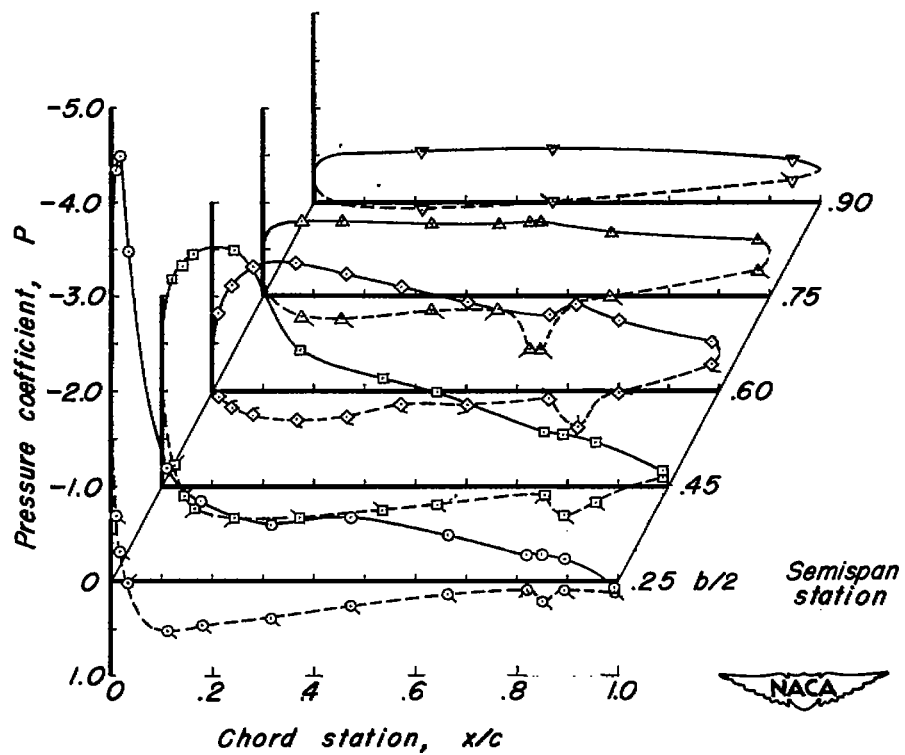
(d) α , 12.5° .

Figure 11.- Continued.



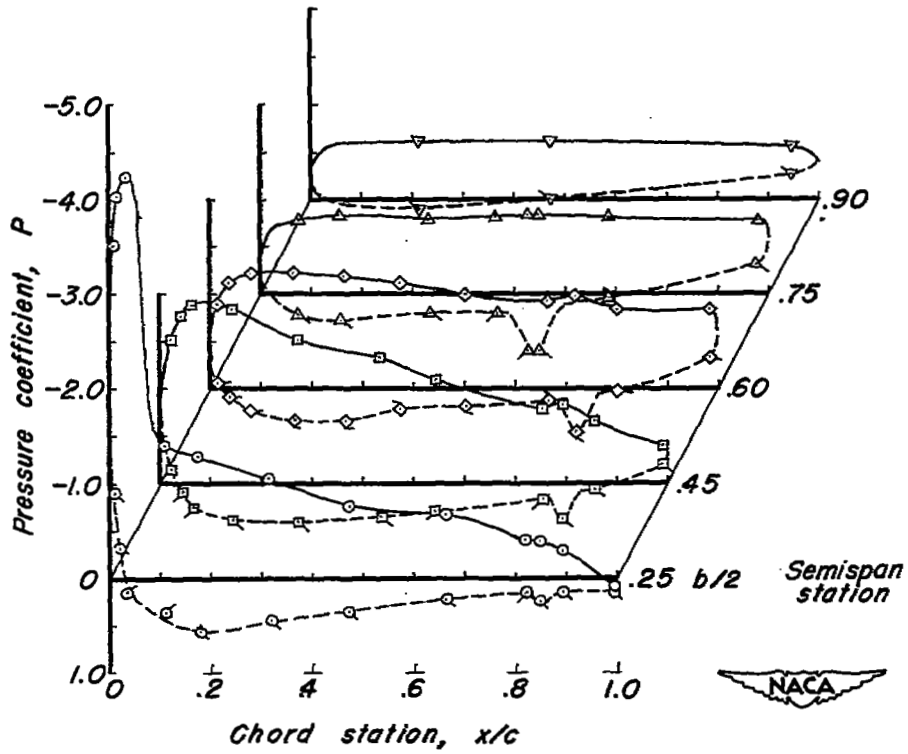
(e) $\alpha, 16.7^\circ$.

Figure II.- Continued.



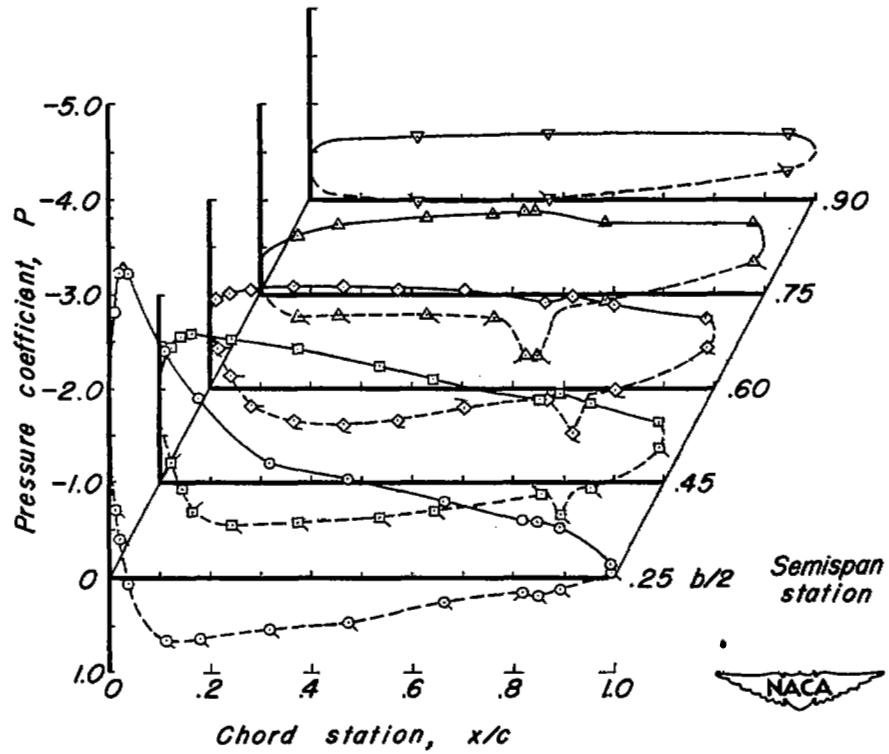
(f) α , 20.8°.

Figure 11.- Continued.



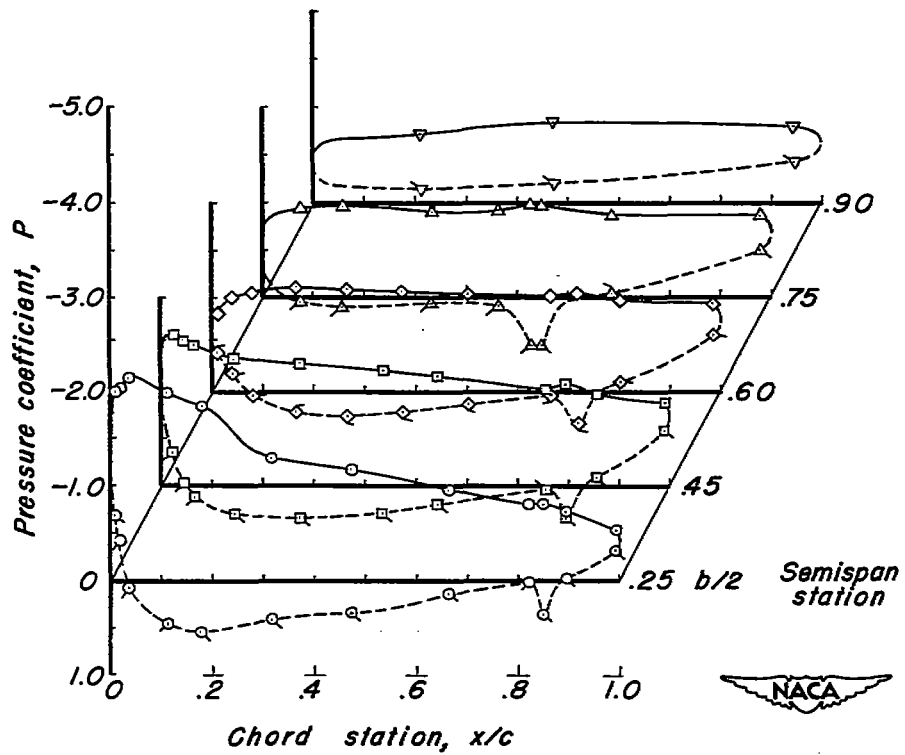
(g) α , 25.0°.

Figure 11.- Continued.



(h) α , 29.0° .

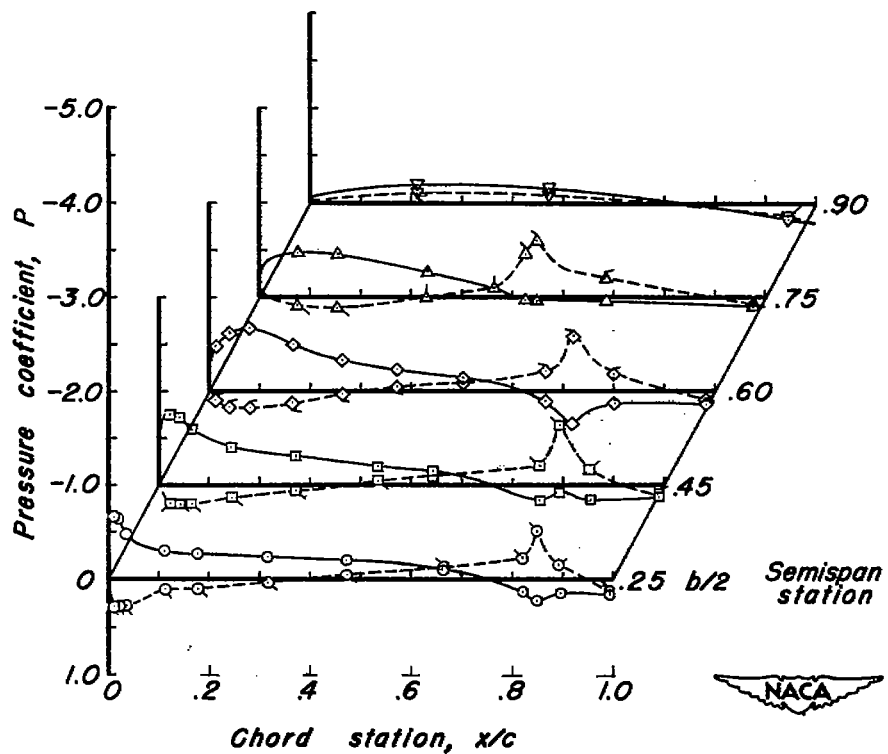
Figure II.- Continued.



(1) α , 33.0° .

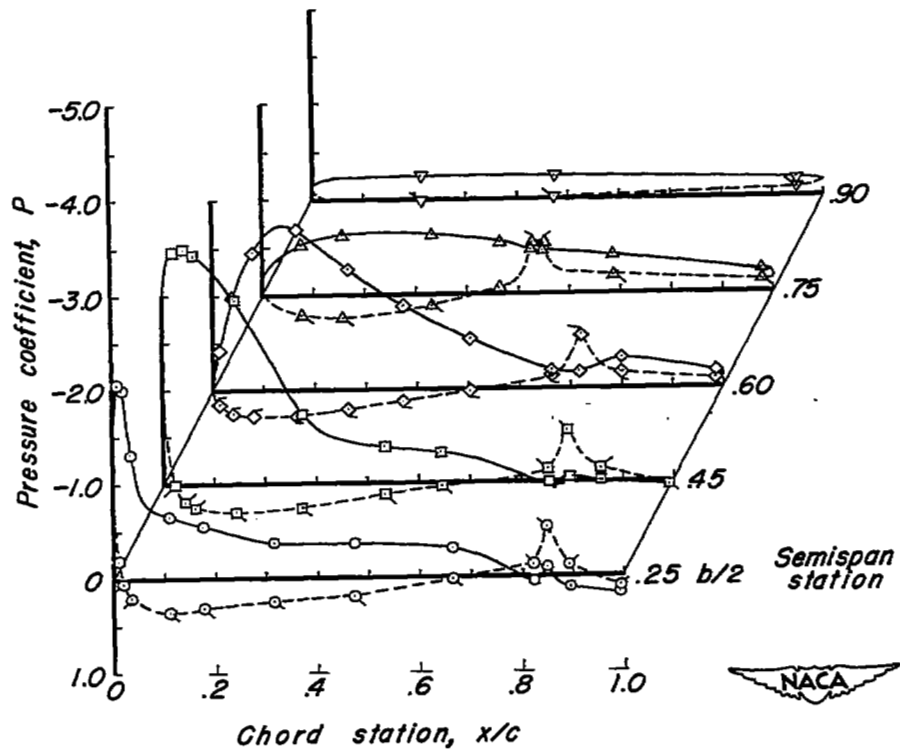
Figure 11.- Concluded.

Flagged symbols and dashed curves
indicate lower surface pressures.



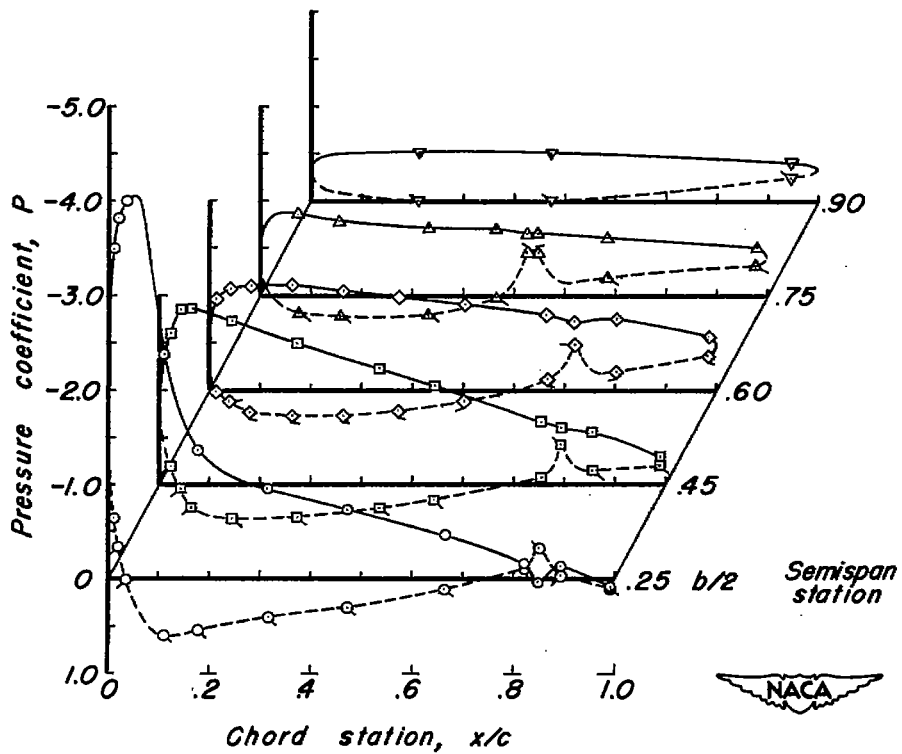
(a) α , 8.1° .

Figure 12.- Pressure distribution along chord for various angles of attack of NACA 65-series wing-body model, trailing-edge controls up 10°



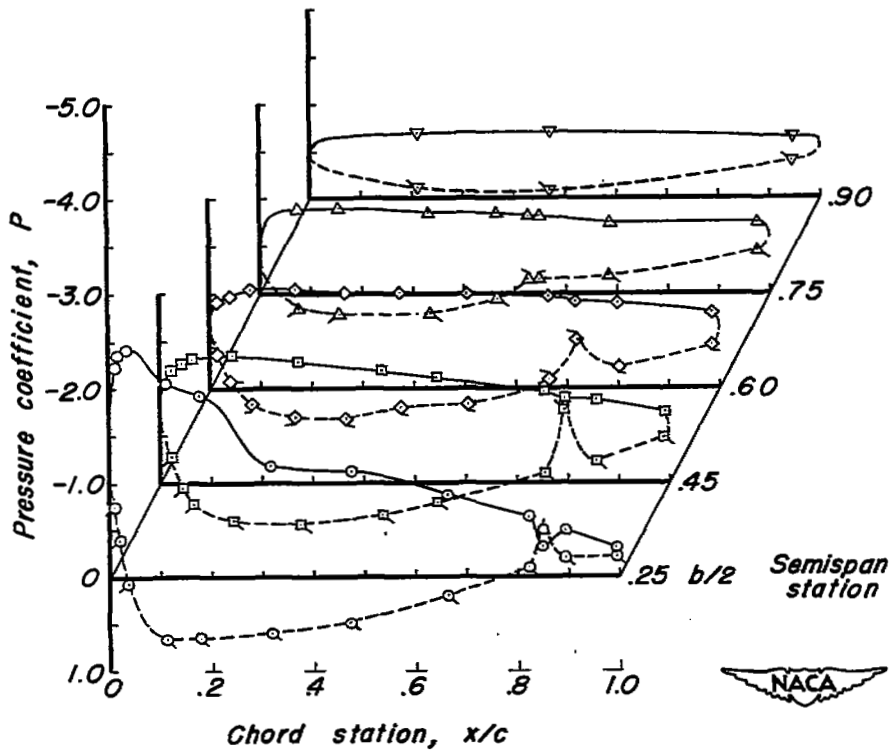
(b) α , 16.5°.

Figure 12.- Continued.



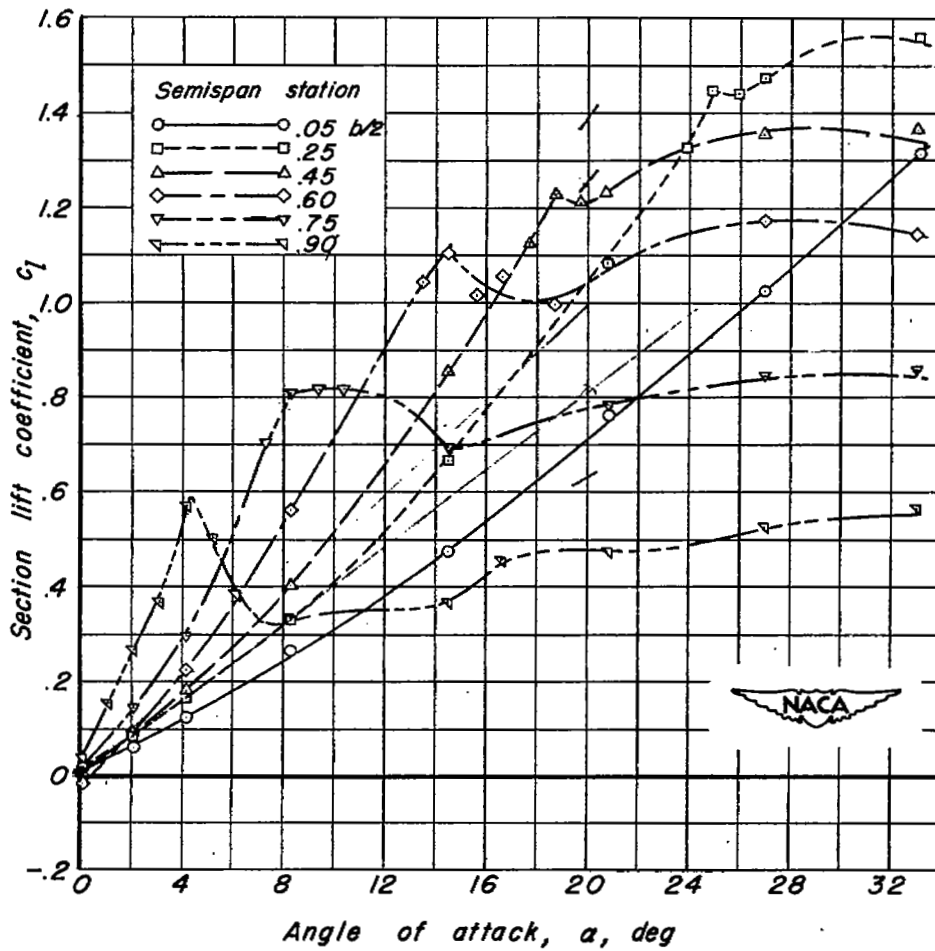
(c) α , 24.8° .

Figure 12.- Continued.



(d) α , 32.9° .

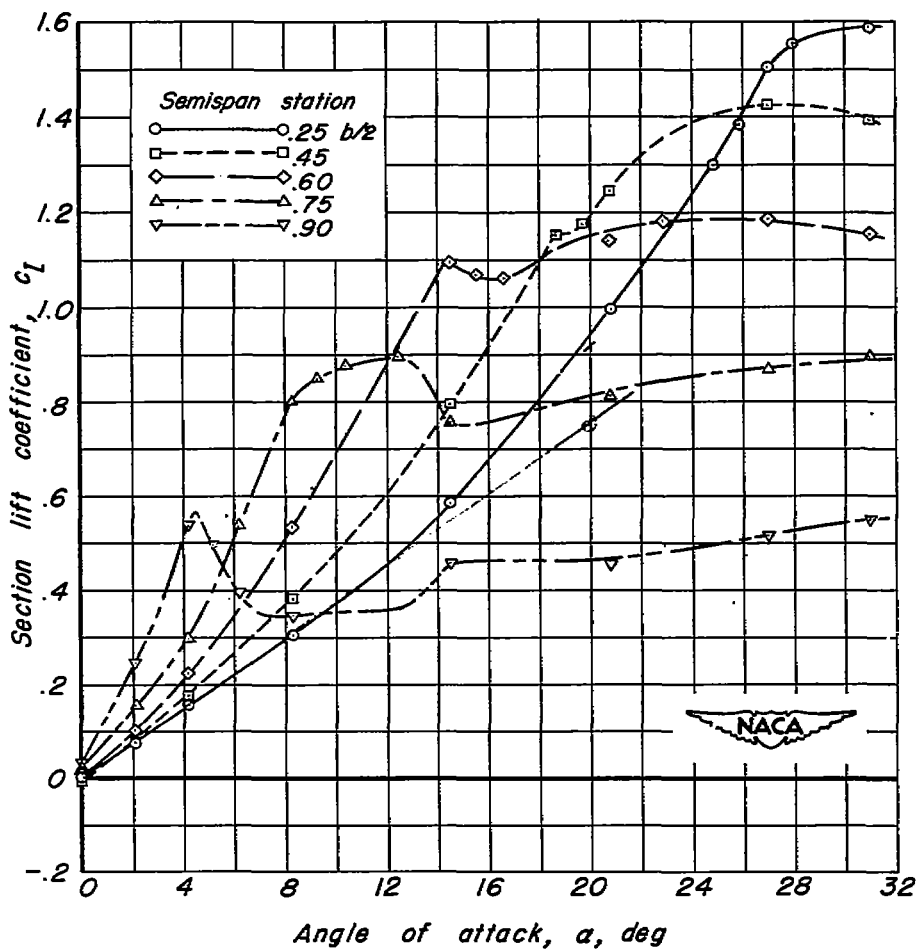
Figure 12.- Concluded.



(a) Modified-wedge wing model.

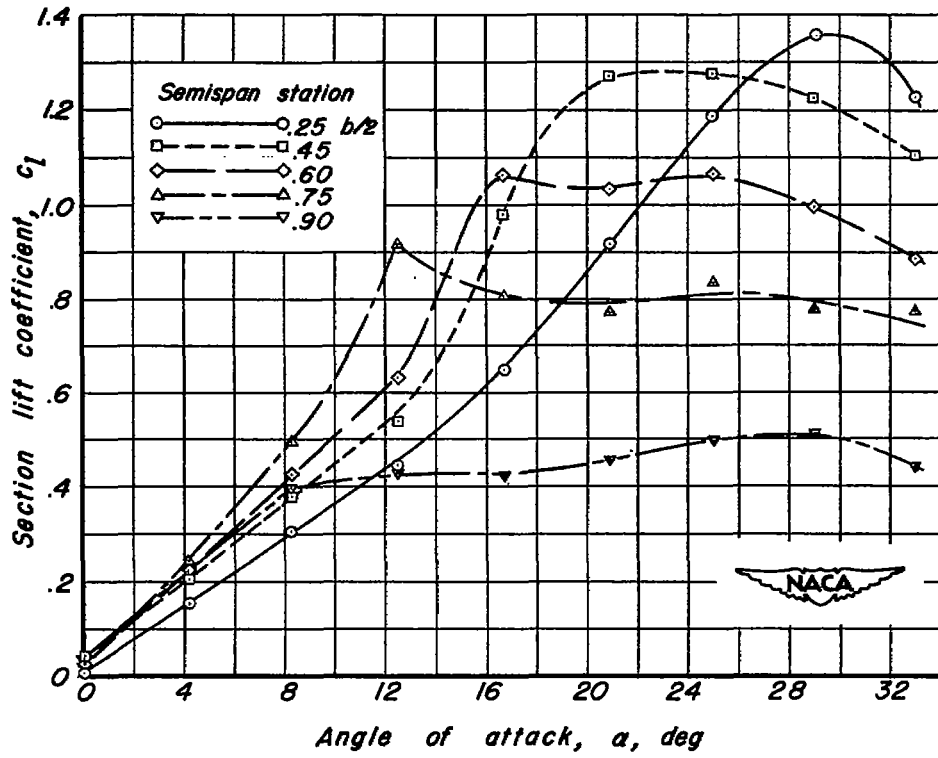
Figure 13.— Section lift curves for several spanwise wing stations.

20070



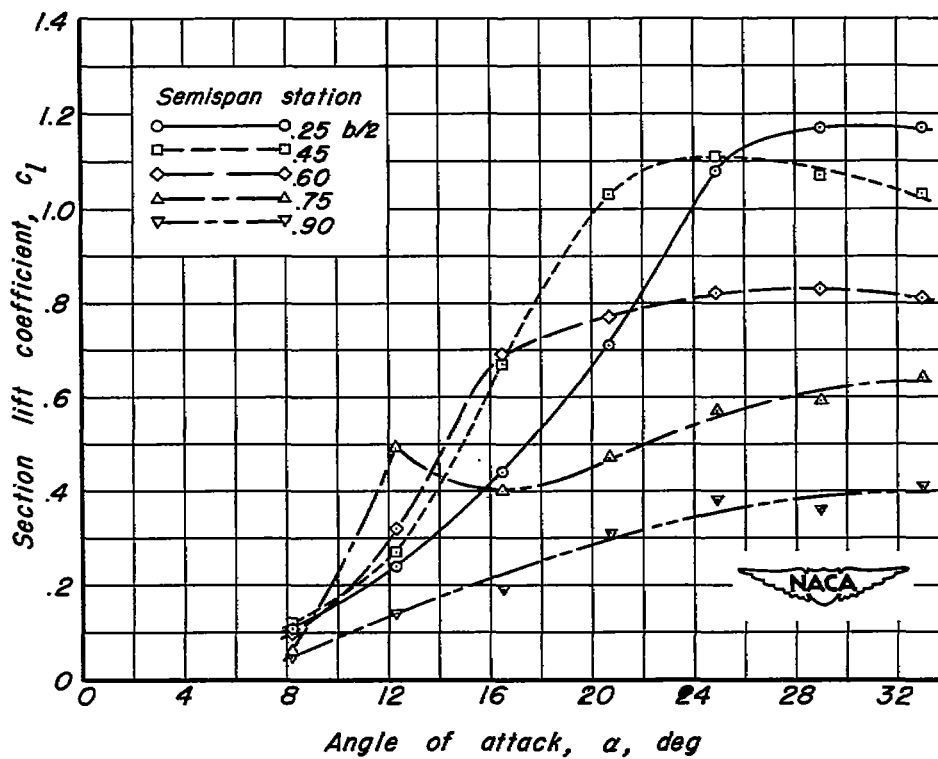
(b) Modified-wedge wing-body model.

Figure 13.- Continued.



(c) NACA 65-series wing-body model, controls neutral.

Figure 13.- Continued.



(d) NACA 65-series wing-body model, trailing-edge controls up 10° .

Figure 13.- Concluded.

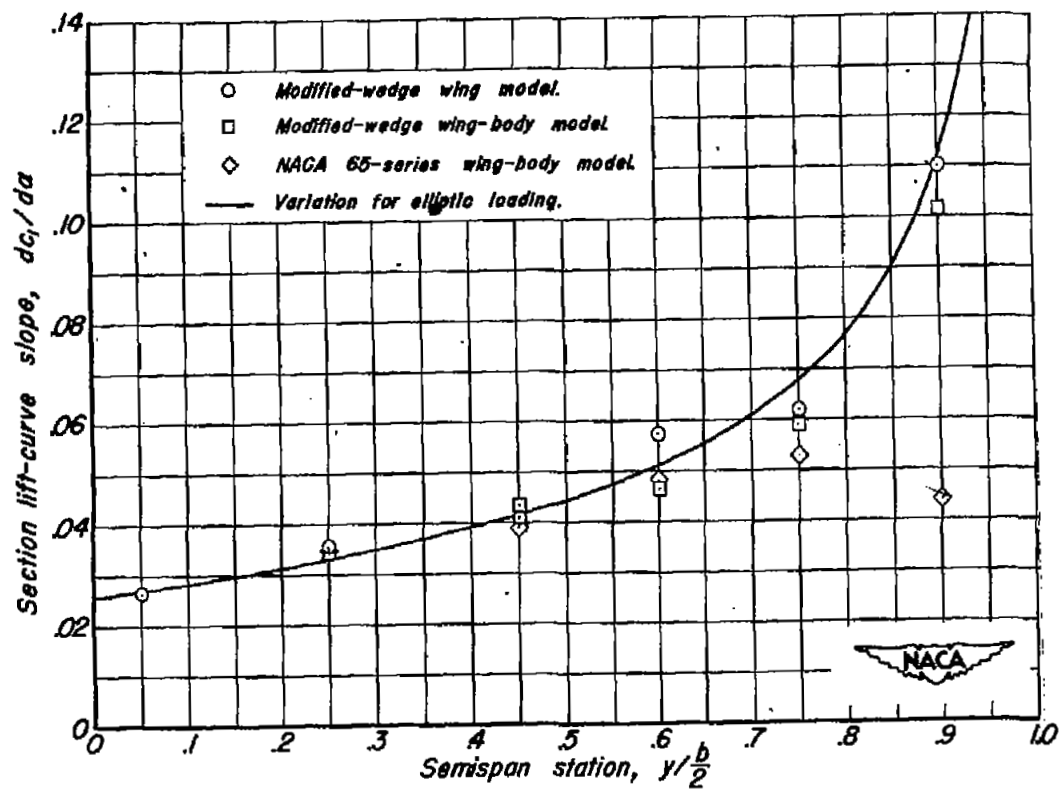
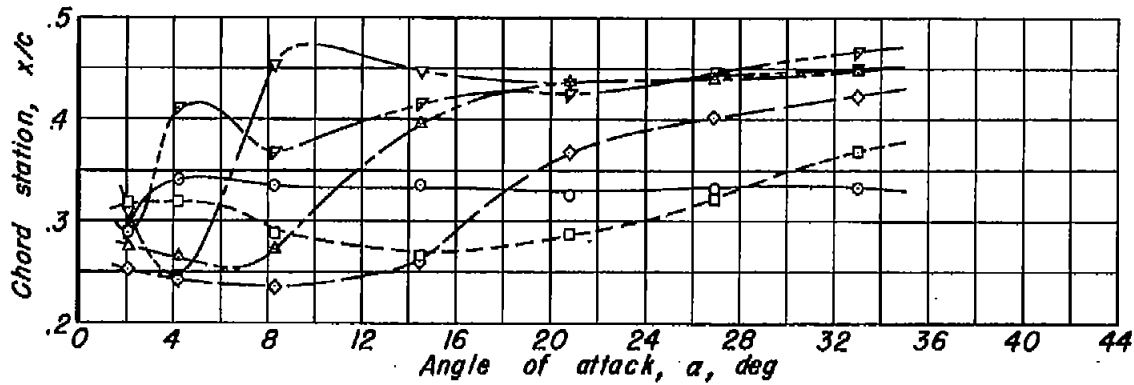
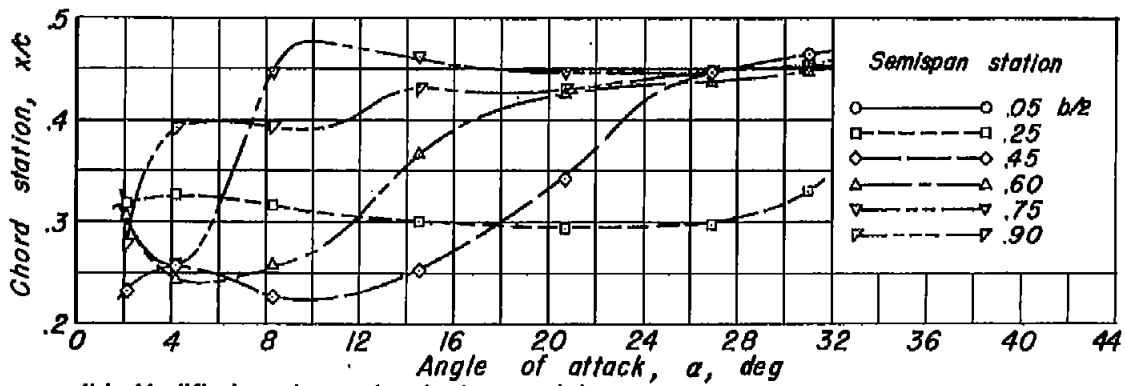


Figure 14.- Spanwise distribution of lift-curve slope through zero lift.



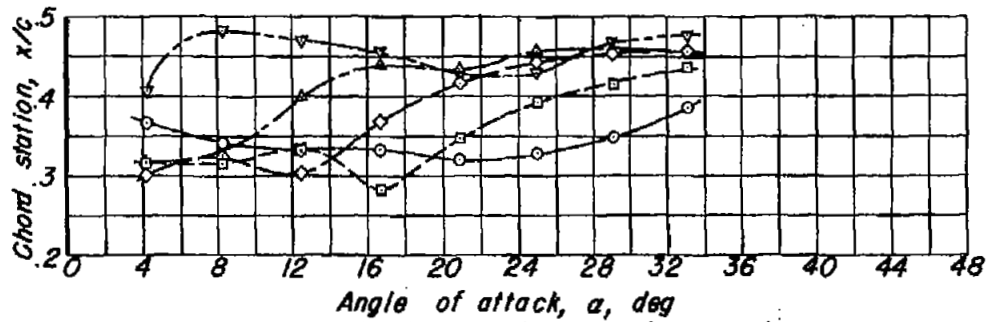
(a) Modified-wedge wing model.



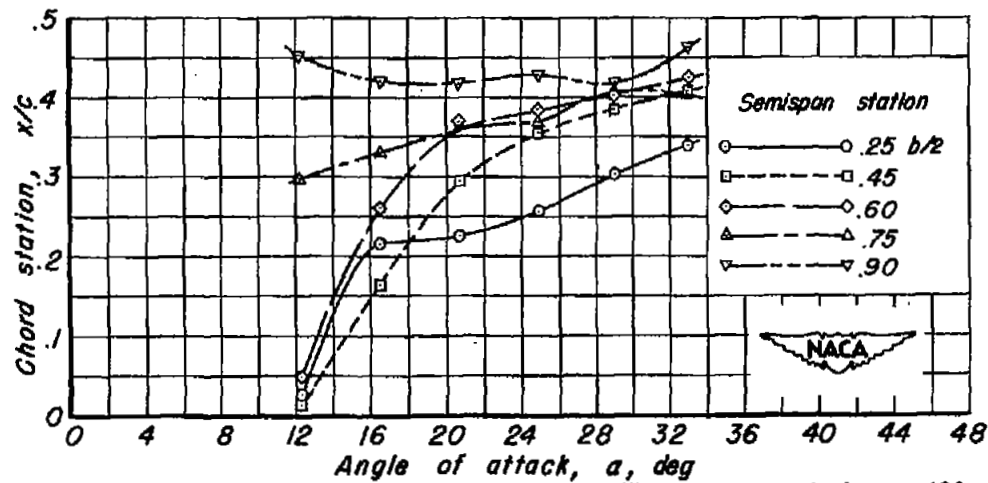
(b) Modified-wedge wing-body model.

Figure 15.- Center of pressure for several spanwise wing stations.



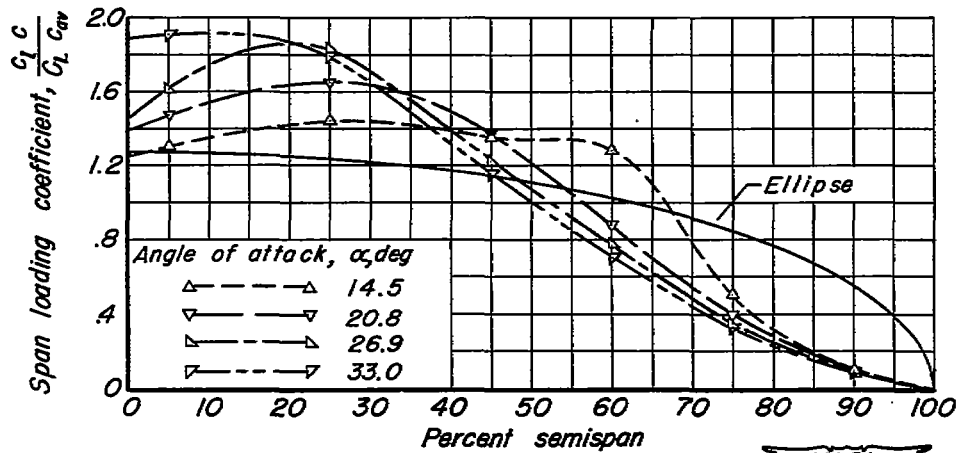
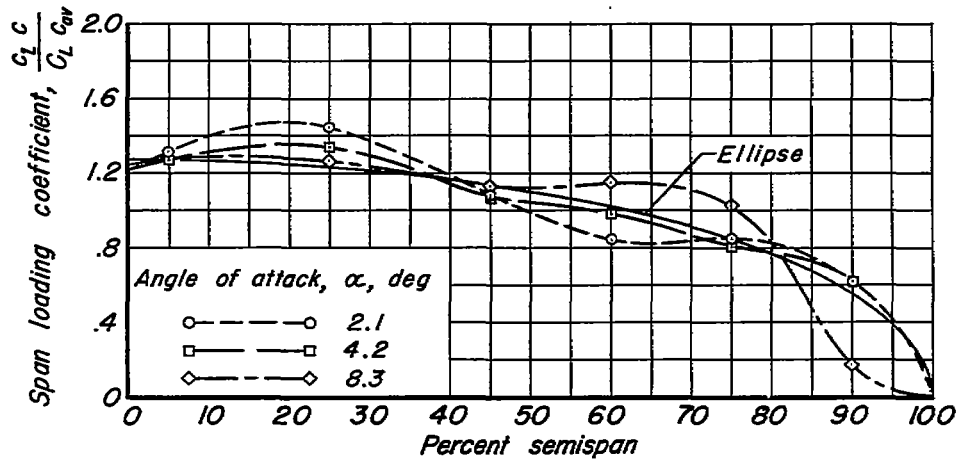


(c) NACA 65-series wing-body model, controls neutral.



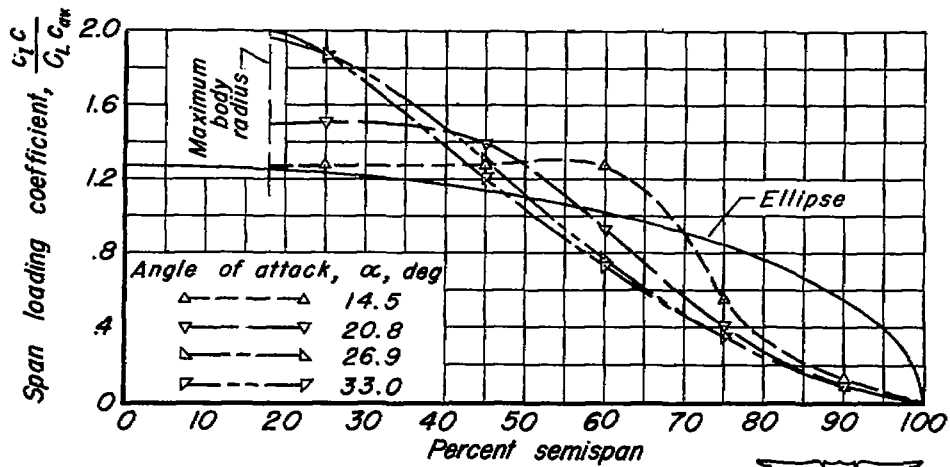
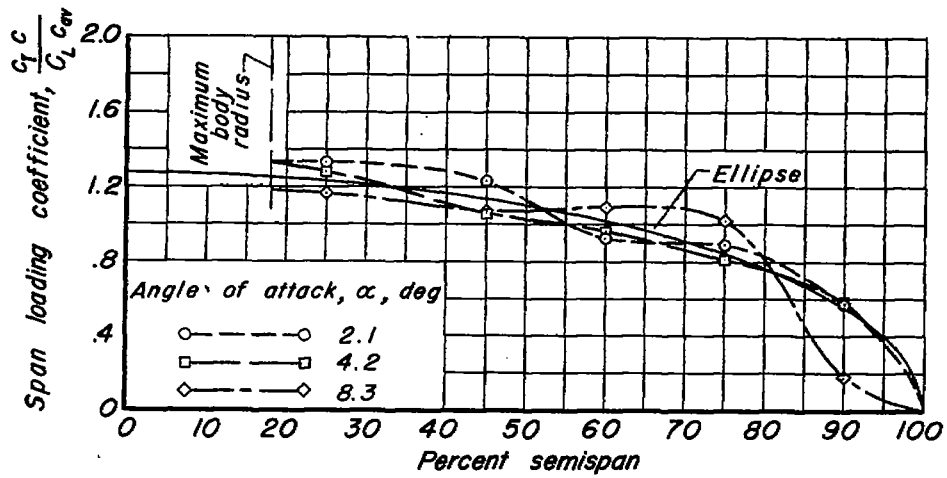
(d) NACA 65-series wing-body model, trailing-edge controls up 10° .

Figure 15.- Concluded.



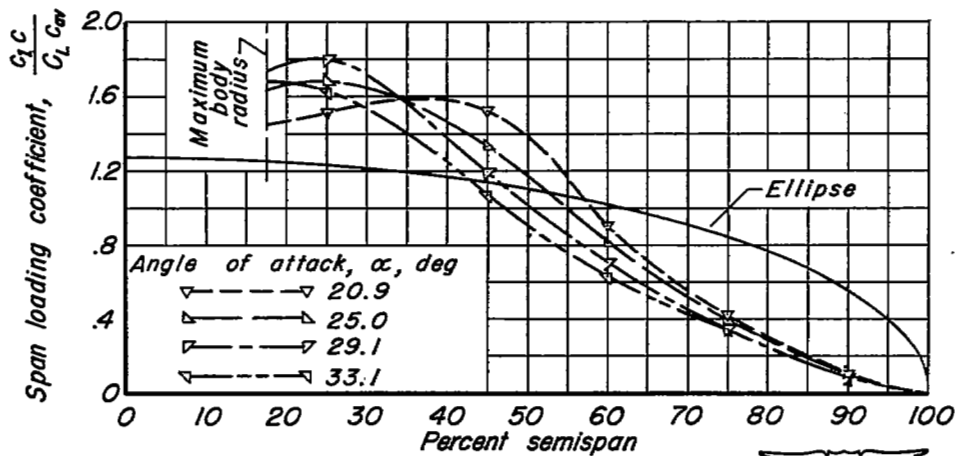
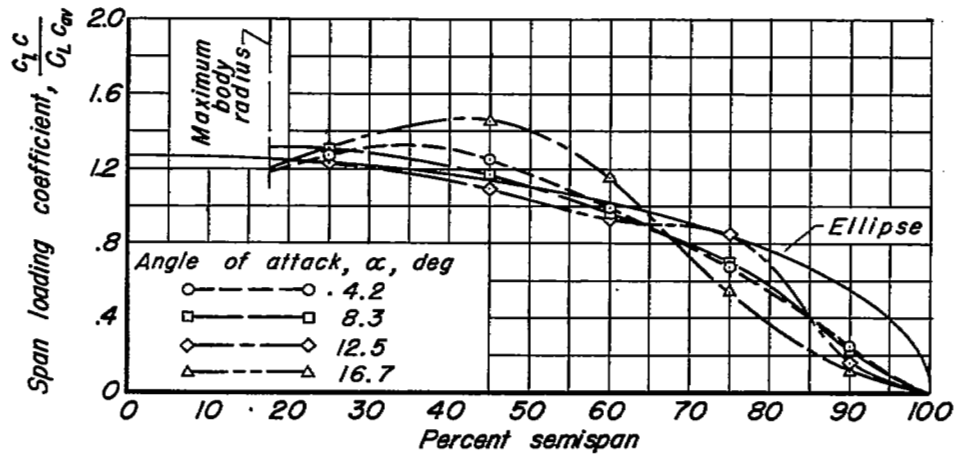
(a) Modified-wedge wing model.

Figure 16.- Span load distribution for several angles of attack.



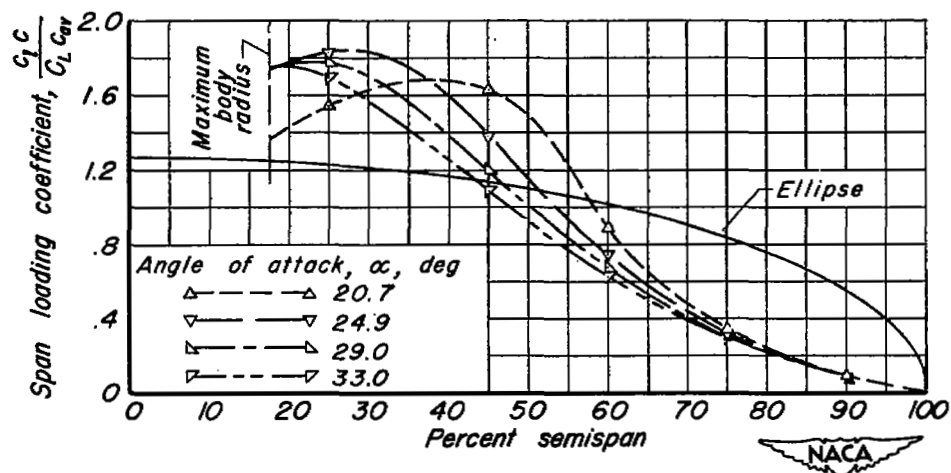
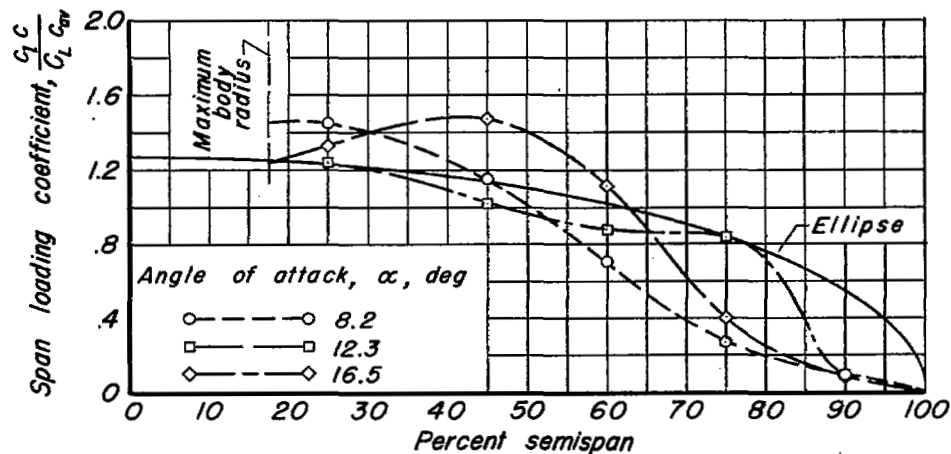
(b) Modified-wedge wing-body model.

Figure 16.— Continued.



(c) NACA 65-series wing-body model, controls neutral.

Figure 16.- Continued.



(d) NACA 65-series wing-body model, trailing-edge controls up 10° .

Figure 16.- Concluded.